THE SPECTROPHOTOMETRY OF THE ORION NEBULA

Thesis by

Manuel E. Mendez

In Partial Fulfillment of the Requirements

For the Degree of

Doctor of Philosophy

California Institute of Technology

Pasadena, California

1964

ACKNOWLEDGMENTS

It is my great pleasure to thank Dr. Guido Münch, my advisor during my four years as a graduate student. His suggestions, criticisms and discussions regarding the thesis work were of mayor importance. I am particularly grateful to him for his ability in delineating to me how astronomical research should be carried out. Finally, his patience and encouragement, during my stay at Caltech, are sincerely acknowledged.

I wish also to show my appreciation and gratitude to Dr. Guillermo Haro, who offered me his confidence and his support throughout the course of my graduate work.

Economical support, at one time or another, was provided by the following organizations:

Observatorio Astronómico Nacional

Instituto Nacional de la Investigación Científica

Organization of American States

Banco de México

I thank Dr. J. B. Oke for providing the photoelectric standard stars in advance of publication. My appreciation goes to all the graduate students who helped at different stages of this work: Bartlett, Chandra, Kellerman and Mihalas. I thank my wife, Marta, for her help in assembling this thesis.

ABSTRACT

The spectral range from λ3600 to λ11 000 has been observed in the spectra of the Orion nebula. The large amount of dust in tle nebula effects the intensity of the lines, according to their wavelengths. The correction, which takes into account this effect, has been obtained using the ratio of the Paschen to the Balmer lines, which arise from the same upper level. The unreddened spectrum-emission lines plus continuum-has been analyzed.

The self-absorption of the Balmer lines has been proven to be non-existent. The Balmer decrement observed is almost equal to that produced by pure recombination. The helium lines indicate small departures from the prediction of the recombination theory. The metastability of the 2^3S level has been investigated, including the ionization of the neutral atom, from this level, by Ly-α quanta. It has been demonstrated that the idea of the exciting star being in the center of the nebula, is consistent with the strengths of the λ3889 lines observed in absorption. Since the self-absorption of the triplet lines of HeI is significant, the H/He ratio has been redetermined. The result indicates a ratio of 11 to 1 (by number).

Since the recombination theory has been found to explain the Balmer decrement, the electron density distribution was obtained from surface brightness determinations

and compared with the densities indicated by the λ3726-29 [OII] lines obtained by Osterbrock in the past. A direct comparison of those two sets of observations has shown that the density fluctuations grow with distance from the center of the nebula. The mass of the nebula is about $30M_{\odot}$ with a probable dust content of about $0.15M_{\odot}$. The latter quantity derived with the assumption that the radius of the solid particles can be represented by an average size of 0.16μ.

With the use of the [OIII] forbidden lines, the electron temperature was determined at several points in the nebula. The distribution obtained clearly indicates that the inner regions are colder than the outer. Since the lines of various elements were observed, an abundance determination was undertaken. The ratio, by number, of He to heavier elements is close to 50, which agrees with the abundance found in the solar cosmic rays. Then by mass, the chemical composition of the nebula can be represented by the following three numbers: X = 0.72, Y = 0.26, and Z = 0.02.

The collision strengths for SII are not well known. Therefore an empirical determination of these parameters is also presented. The ratio of the nebular to auroral lines of [OII] also indicates the existence of density variations. The ratios observed in the nebula have been used to determine the extent of those fluctuations.

TABLE OF CONTENTS

I INTRODUCTION

The physical processes which produce the emission lines in the nebular spectra have been the subject of extensive theoretical investigations. In particular, the problem of the hydrogen and helium lines has been worked out with a high degree of precision. The relative intensities of these lines can be computed accurately for the conditions which might prevail in the gaseous nebulae. Therefore, a comparison of the theoretical results with the observations of nebulae could provide very useful information about the nature of those objects.

As seen from the earth, the Orion nebula is the brightest of all the galactic nebulae; consequently, spectroscopic observations of this object are more easily obtained and the accuracy that can be achieved is of the first order of magnitude. For this reason, a great deal of attention has been devoted to its study by many observers previously. Line intensities have been measured using photographic methods (1,2) as well as photoelectric techniques (3). The energy distribution in the nebular continuum has also been measured, both in the blue(2), and in the red(4). However, the Orion nebula contains an appreciable amount of dust, which weakens the intensity of the lines. The line strengths are effected differentially depending on their wavelengths. Therefore, before attempting a comparison of the observations with the

prediction of the theory, a correction for the extinction produced by dust must be made. And in fact, this reddening correction sets a big limitation. The method used in the past for determining the extinction relies upon the color excesses observed in the Trapezium stars, which can provide the reddening as a function of wavelength. However, this procedure requires the knowledge of the energy distribution in the unreddened continuum of very early type stars. Unfortunately, there is not a single star of early type in the sky unaffected by obscurring material. As a consequence, the reddening corrections derived by this method can not be considered reliable. The Whitford standard reddening curve cannot be used either; simply because it was obtained for stars in HI regions, where the dust might be of a different nature than that imbedded in HII regions.

The space absorption can be more directly estimated by observing the ratio of Paschen to Balmer lines that arise from the same upper level. This ratio is, for all practical purposes, independent of any excitation mechanism, provided that the optical depth at the center of H_α does not exceed 50. A comparison of the observed ratio with that predicted by theory will provide the differential reddening between the two lines. The extinction correction for wavelengths lying in the interval between the Paschen and Balmer lines, can be obtained by interpolation. Using the proper lines, the spectral range that can be covered with our present observational capabilities, extends from $\lambda 3835 (H_{10})$ to

λ10938 (P_δ), a region which contains a large number of important lines. In this fashion, the local absorption is determined, and point-to-point variations of the reddening in the nebula can be easily observed.

Of primary importance is the determination of the nebular Balmer decrement, from which one can decide whether the recombination theory alone can explain the hydrogen emission spectrum or not, and if there is self-absorption, its effects must be taken into account. This question was raised first by Greenstein(2), who pointed out that if sufficient Lyman-α photons are trapped in the nebula, the population of the 2p level might be large, leading to self-absorption of the Balmer lines. There are different ways to estimate the extent of the self-absorption. The simplest one is to compare the observed Balmer decrement with the theoretical one. Another method is to determine the energy distribution in the continuum, if self-absorption occurs there will be a strong emission of two-photon continuum, which can be easily detected at large wavelength. Still another method is provided by the fact that H_α is not observed in absorption in the spectra of the stars imbedded in the nebula. It is possible thus to set an upper limit to the 2p-population, a question which will be discussed in detail in Chapter III.

Once the processes responsible for the hydrogen line formation are determined, it is possible to obtain the electron density from direct surface brightness determinations. If several points are observed, the density distribution

as a function of distance can be obtained. When this distribution is compared with that found by Osterbrock and Flather(5), using the λ3726-29 [OII] lines, some characteristics of possible density fluctuations can be determined. In particular, the ratio of the size of the condensations to the mean distance between condensations, can be calculated as a function of the projected distance from the center of the nebula. The study of this problem is of importance for the understanding of the dynamical processes taking place in the HII regions (6).

Many emission lines of HeI are present in the spectral range from 3800 to 10938. Their relative intensities, as observed in the nebular spectrum, could also be compared with the theoretical recombination values, and in this manner the extent of self-absorption of the He lines can be studied. This problem must be considered before attempting any He/H abundance determination, simply because the self absorption effects, if they exist, would necessarily lead to the overestimation of the He abundance. This mechanism might be significant because the 2^3S level, has in general a much longer mean lifetime than the corresponding 2p level in hydrogen. In fact, the λ3889 of HeI, which arises from that level, observed in absorption in the spectra of several stars imbedded in the nebula, is a direct indication of the metastability of the 2^3S level. The strength of this absorption line has been used by Würm to derive the surface brightness

of the layers in front of the Trapezium stars (7). He found values which are 100 times smaller than those obtained with the emission lines. This fact has led Würm to propose a spatial arrangement of gas and stars, different from the model suggested by the observations of Wilson and Münch(8). He pointed out that in order to fit the λ3889 line observations, the Trapezium stars cannot be in the center of the nebula, but rather they must lie in front of the bright bulk of gas; whereas a layer with much lower electron density, in front of these stars, produces the HeI line in absorption. This new model of the Orion nebula has been criticized by Münch and Wilson (6), pointing out the effects of density fluctuations. More recently, it has been suggested by Münch(9), that Ly-α radiation might be important in the depopulation of the 2^3S level. The Ly-α quanta have enough energy to ionize the HeI atom from that metastable level. Since the density of radiation in Ly-α might be large in the Orion nebula, it would be interesting to consider this new mechanism in the formation of the HeI lines. This problem is presented in detail in Chapter III.

It is well known that the heating of the nebular gas takes place through ionization of hydrogen and helium atoms, produced by the strong ultraviolet radiation field of the exciting star. The stripped electrons, by collisions with each other, establish a thermal distribution. If no cooling mechanisms are considered, the temperature would be close to 60 000 K. However, there are various processes

through which the kinetic energy is converted into radiation that escapes from the nebula. In the case of the diffuse nebula, the most effective processes are: a) the excitation of metastable levels by electron collisions, which are followed by forbidden line emission. Since the rate for second kind collisions, for the electron densities prevailing in diffuse nebulae, is very small compared with the transition probabilities, forbidden line radiation would follow every collosional excitation. Consequently, this mechanism is most important. b) Free-free transitions, which convert the kinetic energy of the electrons into continuum emission, play a certain role in the cooling, but always of secondary importance as compared with the forbidden lines. In particular, OIII, which shows the strongest lines, is the most important ion. However, its abundance, relative to the other stages of ionization, would depend very much on density. When the density is low, the most abundant ion would be OIV, which does not show forbidden emission lines. Consequently, in these regions, the electron temperature would tend to increase. Conversely, when the density is high, OII and OI stages would be more abundant, and although these ions also emit forbidden radiation, the efficiency is not so great as in the case of OIII. Therefore, an increase in temperature, less steep than at low densities, should occur.

Since the existence of density fluctuations has already been established (5), the possibility that temperature fluctuations also occur must be considered.

In addition, the clumping of dust and gas inside the nebula is definitively observed. If the electron temperature is determined as a function of electron density, the role played by dust in the cooling mechanisms might be obtained, provided that accurate theoretical calculations are available. The [OIII] lines, with atomic parameters accurately determined, provide a sound method of determining the electron temperature for various points in the nebula.

Since the line formation processes in nebulae are far simpler than in the case of stars, the abundance determination of various ions with lines in the λ3800-1100 spectral range can be achieved. The uncertainty involved in these analyses is set by the accuracy with which the collisional cross-section may be computed. In some cases, these parameters are not well known. However, the ratio of the helium atoms to the atoms of heavier elements can be determined with uncertainties not larger than 50 percent. Since similar determinations from the solar cosmic rays can now be carried out directly (by means of rocket flights), the analysis of the nebular abundance is of importance. Chapter IV gives the relevant material.

The [OII] λλ3726-29 ratio method for determining the electron density becomes insensitive when this quantity exceeds 2×10^4 cm^{-3}. Therefore, for densities larger than this value, one must rely on the [SII] line ratio, which is sensitive for a much wider range in electron density. Unfortunately the [SII] lines indicate, as a general rule,

densities several times higher than the values derived with other methods. This is undoubtedly due to errors in the collision strengths of the parameters, although there has been some discussion in the past about whether or not such high values might be due to large density fluctuations. If one accepts the possibility that there are large errors in the collisional cross-sections, the Orion nebula can be used as a calibration source, and the relevant parameters can be determined empirically.

Spectroscopic observations of the Orion nebula were carried out during the winter of 1962 at the Mount Wilson Observatory. The discussion and interpretation of part of the material obtained is given in the following chapters.

II

OBSERVATIONAL MATERIAL

The spectrophotometry of the nebular spectra requires the measuring of line intensities in a wide range. In arbitrary units, the intensities lie in a range between 1 to 10^4, approximately. High accuracy can be achieved if both photoelectric and photographic techniques are used. The advantages of the two methods can be combined to increase the efficiency that is obtained with the use of only one of them.

In the present investigation, the two techniques were employed. The photographic spectrograms were obtained mostly with the Newtonian B spectrograph attached either to the 60-inch or the 100-inch telescopes at the Mount Wilson Observatory. A few additional plates were obtained with the X-spectrograph at the Cassegrain focus of the 60-inch telescope. All the photoelectric observations were made with the Ebert scanning spectrometer at the Cassegrain focus (f/16) of the 60-inch telescope.

IIA

THE PHOTOELECTRIC OBSERVATIONS

With the photoelectric cells, it is possible to obtain a linear relation between the luminous energy received at the photocathode and the response delivered to the recording instruments. The high quantum efficiency of the photo-

electric surfaces, compared with photographic emulsions makes the photoelectric spectrophotometry susceptible of yielding a very high accuracy in the intensity measurements of spectral lines. However, that high accuracy, theoretically attainable even for the faintest lines, is restricted in practice by the observation time required to measure all lines with a fixed signal/noise ratio. (This ratio defines the accuracy.) The weaker the line, the longer the time needed to discriminate between signal and noise. As a consequence, a limit for the lowest intensity to be measured was set accordingly. The present photoelectric observations did not go fainter than the intensity 2 in the list published by Flather and Osterbrock(11). The lines with intensities smaller than 2, in the same scale, were measured using photographic methods.

The spectral range covered photoelectrically from λ3500 to λ11000 was observed using two photoelectric cells: the 1P21 was used to measure the region from 3600 to 5100; whereas an S-1 photocathode was employed in the range of wavelengths from 4800 to 11000. The tube was the RCA 7102 operating with 1300 volts.

The scanner employed to make these observations has been described by Oke (11) and only a brief review will be given here. A 600 line/mm grating blazed at 3500 A, in the second order, is the dispersive element. When the red cell - the RCA 7102 - is used, the 1st order is employed, the dispersion being 20 A/mm. An amber filter, which cuts off the wavelength range from 4000 to 5500, is used to avoid the

overlapping second order. When the second order is in operation, the blue cell is used, the dispersion then being 10 A/mm. Again a yellow KZ filter is required at $\lambda>4600$ to cut off the UV third order.

Instead of using an entrance slit, circular apertures were preferred. An entrance aperture of 1.69 mm in diameter was used mainly; however, when better resolution was required, the smallest of the available apertures was used, its diameter being 0.872 mm. At the scale at the Cassegrain focus of 8.3 seconds of arc/mm, and adopting the distance to Orion as 480 pc., those diameters correspond respectively to .0315 pc and .0162 pc in the nebula. Because of its nature, the spectrograph preserves this scale at the exit slit. With no amplification factor, the entrance aperture is projected on the plane of the exit slit with the same size. Then, in the case of the nebula, an extended luminous source, the entrance pupil will determine the spectral resolution. Since the 1.69 mm aperture was used almost everywhere, in the second order a resolution of about 34 A was achieved. The determination of the strength of H_α requires better resolution, since the [NII] lines, at 6548 and 6583, are strong and cannot be neglected. When H_α was measured, the aperture was replaced by one of 0.87 mm, and the exit slit similarly narrowed. Although the λ6583 line is eliminated in this way, a smaller contribution from the 6548 line was also measured and found to be significant. Unfortunately, the 6583 line

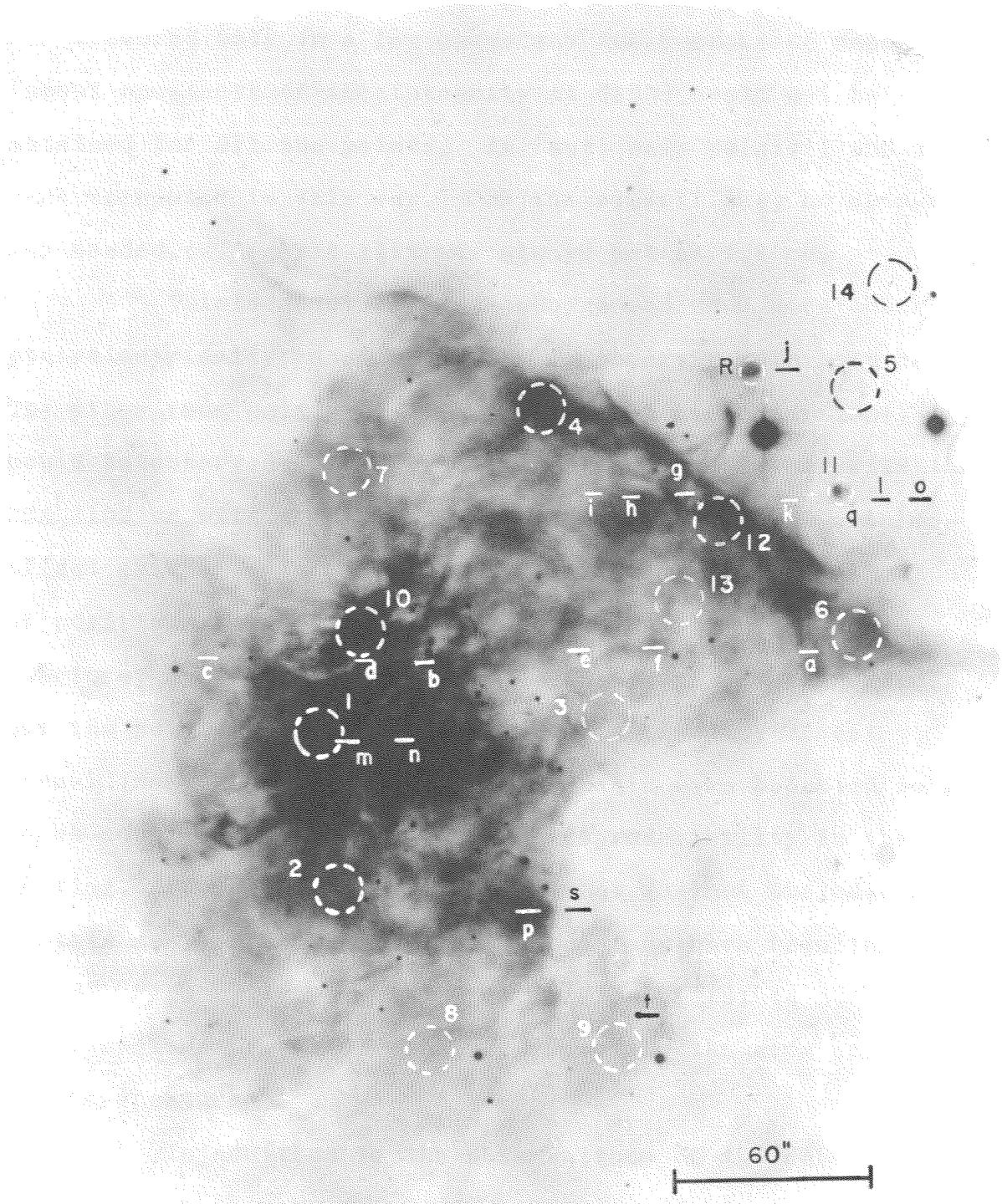

FIGURE 1.

was measured only in a few cases and the correction needed (about one-tenth of the intensity at 6583) could not be obtained for all the points. In fact, only points 1 and 2 were corrected in this way. For the other lines, no change was needed. The exit slit was always set at 1.6 mm.

Thirteen points in the Huygenean zone were observed photoelectrically; nine of them were observed with both cells. The other four points, due to adverse weather conditions, could be observed with only one of the cells, either with the RCA 7102 or with the 1P21. The scanner is equipped with an offset guiding system, but is not suitable for determination of positions. Once the desired point is in the entrance aperture, a field star can be used to assure proper guiding, but the point must have been previously fixed by direct visual inspection. Therefore, the points were selected so as to be conspicuous enough to assure reproducibility in the setting, although for some points, that was not the case and certain scatter in the absolute values may have been introduced. Figure 1* shows the distribution of points observed. The diameters of the circles correspond to the area covered by the apertures.

In addition to the observations of the nebula, it is necessary to make scans of certain standard stars. The instrumental sensitivity, that is the spectral response of the combination telescope-scanner, must be determined. The

*Figure 1 was kindly supplied by Dr. Münoh. Its characteristics have been described elsewhere.

standard stars provide the necessary calibration through a direct comparison of the observations (corrected for atmospheric extinction), with the published results (10),(13). The atmospheric extinction has been studied in some detail by Oke and his data were used for the proper correction. In fact, all the reductions were performed through the use of a program for the IBM 7090, written by Oke. The corrections for both atmospheric extinction and instrumental sensitivity are included in that program.

Three stars were used as standards: γ Gem, α Leo, and ϵ Ori; the first two are in Oke's list (10), whereas ϵ Ori is one of the standard stars of the set published by Code. This star was included for two reasons:

1) The zenith distance is always very close to that of the Orion nebula. Therefore, the calibration is free of large errors arising from differences in extinction.

2) This star has been used by other observers (4), (22), as a photoelectric standard for Orion. Consequently, the comparison of their results with the observations presented here can be better accomplished.

The energy distribution in the continuum of the standard stars is based on the relative spectrophotometry of α-Lyrae, as defined by Code. That system relies upon the calibration of the optical system used in his observations; such a calibration was carried out by the use of

a tungsten ribbon filament lamp (calibrated at the National Bureau of Standards), which was observed through the same optical arrangement as that used for α-Lyrae. Once the calibration is obtained and applied to the monochromatic magnitudes obtained for α-Lyrae, after being corrected by atmospheric extinction, the same star can be employed as a secondary standard. In the list of standard stars given by Oke(10), α-Lyrae has been employed as the calibration source. Although the monochromatic magnitudes of the standard stars obtained in that way have errors not larger than 0.015 mag, they are directly effected by any error present in the absolute calibration. As pointed out by Code (13), errors of the order of a tenth of a magnitude may be present, due to the uncertainties in the primary calibration. Such is the photometric system upon which all the observations are based.

The spectrum of the standard stars was scanned at a rate of 200 A/mm, the speed used by Oke in his observations. The nebular spectrum being a weaker luminous source than the standard stars, was not scanned; it was preferred to set manually the desired wavelength and let the Brown recorder run for a certain period of time. The weaker the line, the longer the recording time. When reducing the observations, a precision planimeter was used to integrate the time variations of the deflections; elimination of the noise fluctuations was achieved in this way. From the consistency of the measurements, such a

procedure provides an accuracy considered not less than 4 percent, when relative intensities are used, viz. the intensity of H_β being unity. In regard to the absolute value of the flux received, that is not the case. The mean error for points as numbers 7, 3, 5, is on the average not less than 12 percent.

The measurements of the other points (more conspicuous) have a mean error of less than 8 percent, on the average. These larger errors are undoubtedly due to variations in the position of the entrance aperture on the nebula. Those errors are also affected by the absolute calibration mentioned above. Therefore, the errors on an absolute basis might be quite appreciable.

Surface Brightness Determination

Due to the intrinsic linearity of the photoelectric methods, the deflections obtained in the paper recorder at any wavelength, can be immediately converted to absolute energy units, provided that the energy-deflection relation is given by absolute calibration. The photometric system, as set by Code, defines the calibration value as follows: at the effective wavelength of the V filter (λ_e = 5560A), a star of apparent magnitude V = 0.0, and B-V = 0, produces a monochromatic flux of 3.8×10^{-9} erg/cm^2/sec/ $\bar{A}$. Since the energy distribution for the standard stars is given, monochromatic fluxes, in absolute units, may therefore be derived at any wavelength. Consequently, the deflections obtained

when scanning the standard star spectra provide the relation energy-flux to deflection needed to calibrate the instrumental scale. Intensities, in absolute units, can now be easily obtained for the lines of the nebular spectrum.

The determination of the surface brightness in some particular hydrogen line is of theoretical importance, as it is discussed in Chapter III, the so-called emission measure, $N_e^2 \ell$, can be derived directly from the surface brightness value, provided that the line can be assumed to be produced by pure radiative recombination.

The actual star used for the calibration of the monochromatic magnitudes was Υ Gem ($M_V = 1.95$); after reduction it was found that at $\lambda 5060$, with a 15.5 A band-pass, the instrumental magnitude (or the deflection) was 1.84 ± 0.011. This value can be related to the actual flux through the calibration value of the photometric system. Since for a AOV, as α-Lyrae, we have the relation (per unit $1/\lambda$ interval)

$$1.052\ F\ (5560) = F\ (5060) \quad ,$$

then for Υ Gem, with V = 1.95 we obtain for the band-pass of 15.5 A (the width of the exit slit), the relation:

$$1.84\ \text{mag} \equiv 123.6 \times 10^{-10}\ \text{erg/cm}^2\text{/sec} \quad .$$

Of the observed points in the Orion nebula, number 1 is the brightest and very easy to locate; correspondingly, the scatter in the absolute value of the flux observed for that point is very small. The instrumental magnitude is 6.80 ±0.11. The flux received, at λ4861, is then given by:

$$F(H_\beta) = \frac{123.6 \times 10^{-10}}{10^{0.4(6.80-1.84)}} = 1.22 \times 10^{-10} \text{ erg} \cdot \text{cm}^{-2} \text{sec}^{-1}$$

The surface brightness is obtained by dividing this value by the solid angle, at the telescope, subtended by the area observed. If d is the diameter of the entrance aperture, in seconds of arc, the solid angle is given by

$$\Delta\omega = \frac{\Delta S}{r^2} = \frac{\pi d^2 \left(\frac{\pi}{180}\right)^2 \left(\frac{1}{3600}\right)^2 r^2}{4r^2}$$

$$\therefore \quad \Delta\omega = 1.86 \times 10^{-11} \, d^2 \quad \text{steradian.}$$

With the 0.169 aperture, the surface brightness is then

$$S_\beta = 0.035 \pm 0.003 \text{ ergs/cm}^2\text{/sec/steradian} \; .$$

The same quantity has been determined in the past by: Ambartsumian(13) who found a value of 0.022; Stromgren (14) who obtained a much higher value of 0.160 and, more recently by Wurm and Grubissich(15) who derived a value 0.032 in perfect agreement with the present determination. A similar procedure provides the surface brightness for the other points. Table I shows the results. It must be pointed out that, before interpreting in terms of a physical theory,

those values should still be corrected, since the extinction produced by the dust inside the nebula has not been taken into account. Therefore, the true values are larger than the observed ones.

TABLE I

Point	$S_\beta \times 10^3$ ergs/cm^2/sec/steradian	$S_\beta \times 10^{-3}$ Rayleighs
1	35.2	102
2	20.1	61.5
3	10.0	30.8
4	22.3	68.6
5	2.9	8.9
6	14.4	44.3
7	11.2	34.8
8	9.5	29.4
9	6.2	19.3
10	26.1	80.7
11	10.7	32.9
12	22.8	70.0
rim	6.4	19.9
13	9.0:	27.8

c) The Reddening Correction

Dust inside the nebula absorbs and scatters light. Therefore, the wavelength dependence of the extinction, produced inside the nebula, must be known in order to estimate the reddening correction to be applied to the various emission lines observed. A great deal of work, from part of the

observers, has been devoted to the comparison of pairs of stars of the same spectral type showing various amounts of reddening. It is now generally accepted that all stars not imbedded in HII regions, show a unique law of interstellar reddening. However, Divan(17) has proposed that the same law holds everywhere if the variations of the classical reddening law, clearly shown by the stars in the neighborhood of emission nebulae, are the direct result of peculiarities in the continuum spectra of these stars. This interpretation is difficult to accept, because uniqueness of the extinction law would require the same nature of the dust particles everywhere. Although, according to the theoretical work, the reddening law is fitted by a large variety of particles, the larger radiation pressure, present in the HII regions, would certainly affect the mechanisms of growth and destruction of grains. Furthermore, little is known about the energy distribution, in the blue, for early type stars. To speak of peculiarities is then meaningless.

On the basis of these objections, the existence of a regional law for extinction for the Orion nebula has been preferred.

Some recent spectrophotometric investigations of this nebula have used the six-color photometry of the Trapezium stars to estimate the amount of nebular reddening. The extinction values derived in this fashion have been obtained by Mathis(1). However, he derived the correction by computing the integrated magnitude of four stars with the

same spectral types as the Trapezium stars, but unreddened. The differences from the observed values, as given by Stebbins and Whitford(19), are the corrections. In this way, the largest weight is given to θ^1C(06), the brightest but not the most reddened of the four. Furthermore, there is not a single 06 star in the sky which is not reddened; therefore, there is not a priori procedure to determine the distribution of energy in the continuum spectra of early O stars. The theoretical atmosphere models could provide the unreddened standard, but unfortunately there is a large disagreement among the various numerical results, and for the time being, this possibility must be ruled out. Clearly, the corrections derived in this way do not represent the nebular extinction everywhere throughout the nebula. In fact, the results obtained in this work, as well as recent observations by Mathis himself(20), prove beyond any doubt that a larger reddening than the one derived from the photometry of the stars is present in the Orion nebula.

A more direct estimate of the nebular reddening can be obtained using the ratios of the intensities of the Paschen and Balmer lines arising from the same upper level. This method is based upon the assumption that the hydrogen emission lines are produced by a pure recombination process. The computations, carried out by Burgess(21), which take into account the orbital degeneracy of the hydrogen atom, provide the theoretical Paschen to Balmer ratios to be compared with the much larger observed ratio values. The existence of

self-absorption processes, in addition to the radiative recombination mechanism, might effect the validity of the method since the P/B ratios are directly effected. The relative importance of the effects produced by self-absorption, as well as those caused by collisional excitation, will be discussed in Chapter III.

Two pairs of lines were used in the derivation of the reddening correction: the two lines arising from level n = 6; λ10938 and λ4101, and the pair originating from level n = 9; λ9229 and λ3835. Those four lines are fairly strong and free of blending lines, a difficulty that prevents the use of other lines, viz. λ3888 blended with the heI line at λ3889, 3970 blended with [NeIII] λ3965, etc. Fortunately, the atmospheric molecular absorption does not affect, in a significant way, the intensities of the relevant Paschen lines λ10938 and λ9229, provided that the relative humidity is not too high.

The actual procedure is best illustrated by an example. Table II shows the numerical steps used for the reddening determination for point 1, which was observed oftener than the other points.

TABLE II

COMPARISON OF PASCHEN AND BALMER LINE INTENSITIES

1 Balmer Line	2 Intensity (H_β=100)	3 Paschen Line	4 Intensity H_β=100	5 Theor. Ratio (21)	6 Observed Ratio	7 Reddening (mag)	8 Mathis Red
4101	14.9	10938	70	0.329	4.9	2.88	1.72
3835	3.10	9229	14	0.351	4.5	2.78	1.40

Column 7 gives the amount of light lost due to differential selective absorption in the spectral interval bounded by the corresponding lines. The reddening correction at other wavelengths can be interpolated from those values. If for pure numerical convenience we set the absorption at H_β equal to zero, we can see that, in an extinction vs. wave number diagram, those values define two straight lines of slightly different slopes. Theoretical investigations(22) indicate that the reddening curve must be convex; upward at the infrared and downwards on the ultraviolet side. The slopes of the lines do not disagree with that proposed shape; therefore, the points obtained are fitted to a similar curve. The result is displayed in Figure 2, where the curve derived by the six-color photometry of the Trapezium stars is also plotted. If the six-color photometry had not underestimated the reddening in the ultraviolet, as seemed to be the case, the curves would look much more alike. The points on the P/B curve correspond to the wavelengths of the corresponding

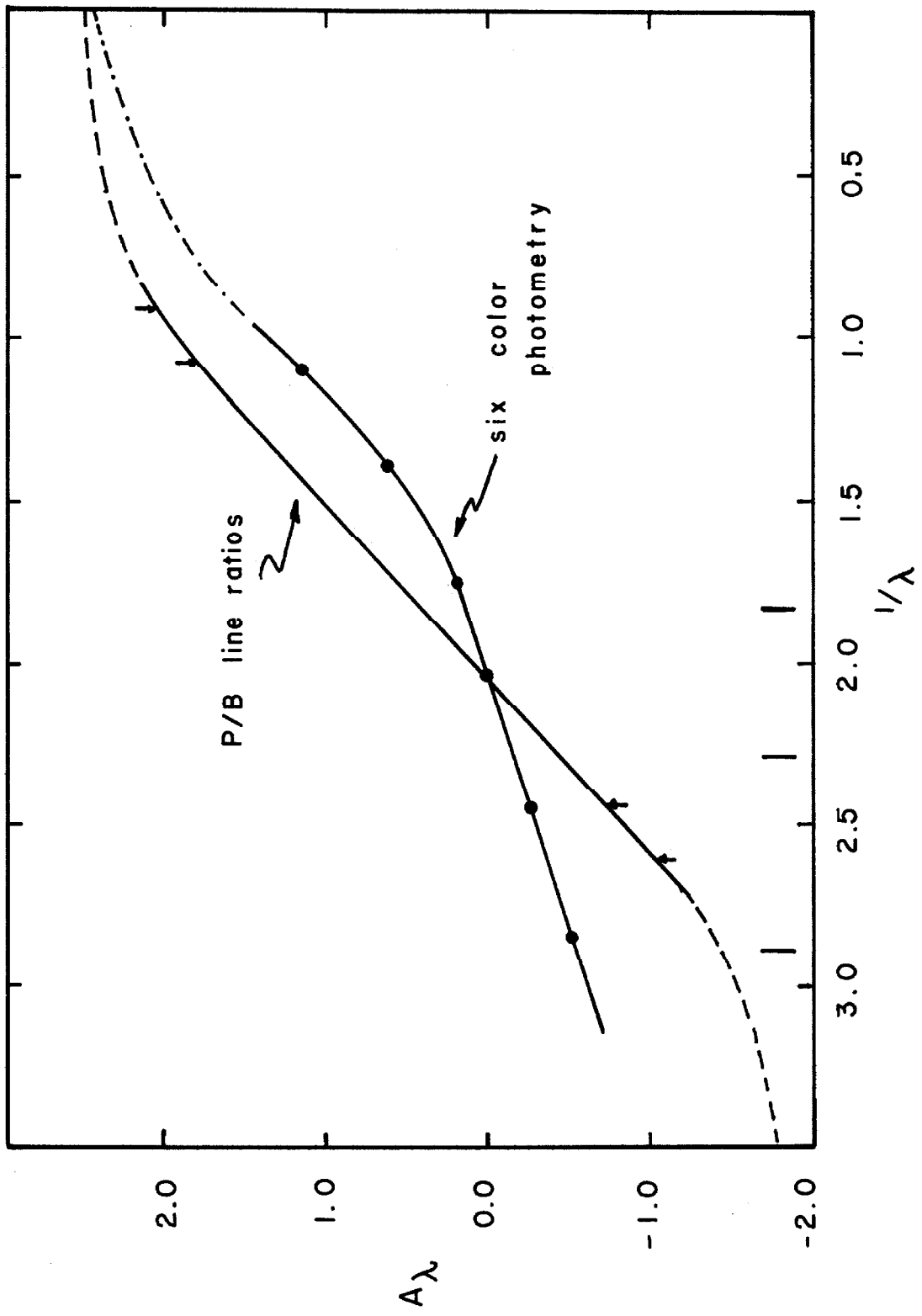
P/B line ratios
six color photometry
2.0
1.0
0.0
-1.0
-2.0
A_λ
0.5
1.0
1.5
2.0
2.5
3.0
$1/\lambda$

Figure 2.

H lines used. The vertical lines indicate the inverse of the effective wavelength of the U,B,V-system.

The linear part of the curve can be represented by the equation:

$$A_V = 1.87\ (1/\lambda) + cte,$$

the slope of the line being in excellent agreement with the results obtained by Baade and Minkowski(18). However, this method of determining the reddening curve could neither prove nor disprove the existence of a small curvature in the neighborhood of λ4300, as present in the Whitford curve.

The reddening correction for the other points was determined in the same way. For the points that were not observed with the two cells, the correction was derived by the intensity of H_δ and H_{10} in the blue; and with the intensities of the Paschen lines, 10049 and 9229, when observations were carried out with the red cell only.

Errors in the instrumental sensitivity function or improper correction for the atmosphere extinction would tend to affect directly the reddening determination. Although the mean errors, as mentioned before are less than 4 percent, and mostly due to extinction, it is possible that some systematic errors in the response of the instrument are present; such possibility is suggested by the discrepancy with the data of Mathis(20) and Aller(3). ε Ori has been one of the standard stars of Code used by the two latter observers, and since some observations of the same star were carried out for the present work, we can compare our results with those

TABLE III

ε Ori

$1/\lambda$	Code	This Work
	Magnitudes	
0.926		0.87
1.005	0.98	0.82
1.09	0.80	0.79
1.14	0.72	0.64
1.25	0.56	0.50
1.34	0.42	0.38
1.50	0.27	0.21
1.65	0.14	0.13
1.72	0.07	0.07
1.80	0.00	0.00
1.97	-0.10	-0.11
2.18	-0.17	-0.20
2.39	-0.30	-0.32
2.48	-0.36	-0.37
2.59	-0.40	-0.39
2.74	-0.42	-0.43
2.94	-0.44	-0.54
Mean error		±0.018

Wavelength	Point 1		Point 2		Point 3		Point 4		Point 5	
					HYDROGEN LINES					
10938	70	10.0	94	10.2	154	9.6	85	10.4	60	9.9
10049	38.5	5.8	41	7.0	56	5.9	40	6.0	-	-
9229	15.8	3.3	16.6	3.5	22.2	3.3	14.1	2.8	Too weak	
8862	4.6	1.0	-	-	11.1	1.4	-	-	Too weak	
6562	642	269	695	268	860	258	780	300	730	300
4861	100	100	100	100	100	100	100	100	100	100
4340	32.6	47.6	34	48.7	26.1	46.0	32.1	47.5	32.9	46.8
4101	14.9	29.4	16.3	30.3	12.3	30.0	13.5	28.0	17.1	29.8
3970	11.5	27.	11.0	23.1	-	-	9.4	21.8	-	-
3889	7.0	15.7	6.5	14.5	5.8	18.1	6.0	15.2	-	-
3835	3.5	9.4	3.6	8.4	2.7	8.8	2.9	7.9	-	-
3798	2.3	6.6	2.9	6.9	-	-	2.7	7.4	-	-
pg3770:	1.9	5.3	1.9	4.5	-	-	-	-	-	-
3750	1.2	3.7	2.0:	6.1	-	-	-	-	-	-
					HELIUM LINES					
10830	302	43.0	550	50.0	689	608	315	44.8	180	36.0
7065	240	8.5	-	-	38.0	6.4	27	7.9	-	-
5876	18.0	9.8	15.9	9.4	26.5	11.3	23.0	11.5	13.2	7.8
4471	3.0	3.9	3.3	4.2	3.0	4.5	3.2	4.5	3.9	5.1
4026	3.1	2.4	1.2	2.2	1.0	2.9	1.1	2.5	-	-
*3888	-	2.7	Ext.	1.3	Ext.	4.9	Ext.	2.0	-	-

*Extrapolated

T A B L E I V

Point 6		Point 7		Point 8		Point 9		Point 10		Point 11	
85.0	10.0	78	10.5	93	10.7	92	10.6				
48.0	6.5	53.0	7.4	44	6.5	47	6.9				
21.3	3.4	22.5	3.7	18.9	3.3	18.9	3.5	-	-	-	-
-	-	-	-								
800	280	745	260	818	300	810	290	-	-	-	-
100	100	100	100	100	100	100	100	100	100	100	100
28.9	46.7	28.9	45.8	29.4	46.0	28.8	47.5	29.5	45.0	27.5	44.0
14.2	29.9	14.4	30.4	14.6	30.0	14.7	30.0	14.5	28.9	14.8	31.0
8.7	21.0	10.5	25.6	9.8	23.0	9.8	22.8	10.1	23.0	-	-
6.5	19.3	7.3	18.9	7.4	18.7	6.0	15.0	6.6	16.2	-	-
3.2	9.2	3.1	9.0	3.2	9.6	-	-	3.0	8.2	-	-
1.7	5.3	2.3	6.7	2.2	6.6	-	-	1.8:	5.0	-	-
-	-	-	-	-	-	-	-	-	-	-	-
-	-	-	-	-	-	-	-	-	-	-	-
274	38.0	600	62.1	467	58.6	408	54	-	-	-	-
-	-	-	-	-	-	27.	8.9	-	-	-	-
19.6	9.5	21.4	11.0	18.7	9.7	23.3	11.7	-	-	-	-
2.7	3.8	2.7	3.8	3.2	4.4	2.8	3.9	2.9	3.9	2.6	3.8
1.0	2.1	1.1	2.5	1.3	2.8	-	-	1.1	23.7	-	-
-	4.0	Ext.	5.2	Ext.	5.3	Ext.	1.8	Ext.	3.0	-	-

A B I

Wavelength	Point 1		Point 2		Point 3		Point 4		Point 5		Point
					O III LINES						
5008	383	357	345	315	350	305	250	225	158	148	.70
4959	122	115	108	106	110	102	80	78	48	37	52
					O II LINES						
7325	23.5	7.6	33.8	9.2	38.9	8.1	36.6	10.1	-	-	5.1
3728	39.0	129	82.0	215	27.0	190	71.0	206	97	230	.5
					NE III LINES						
*3967	Ext.	7.5	Ext.	3.9	-	-	Ext.	2.6	-	-	t.
3868.7	9.9	23.2	4.8	11.2	-	20.1	4.2	9.5	-	-	54
					S III LINES						
9532	500	83.0	728	140	329	34.0	398	69.0	312	75.0	33
9069	177	33.0	172	40.5	265	32.0	171	31.0	59	12.0	10
					S II LINES						
6724	9.5	3.8	19.4	6.8	1.5	0.6	36.6	13.5	-	-	.6
4072	1.5	3.2	1.0	1.7	-	-	1.2	2.7	-	-	.2
					A III LINES						
7135	24.8	8.2	34.8	12.3	36.6	8.3	32.5	10.5	14.3	9.0	.9

*Extrapolated

\ B L E I V

Point 5		Point 6		Point 7		Point 8		Point 9		Point 10		Point 11	
158	148	.70	152	308	282	310	268	262	236	309	270	98	88
48	37	52	49	102	96	92.8	87.5	83.8	79.7	101	91	29	27
-	-	5.1	9.2	34.1	9.2	29.4	8.2	35.6	10.1	-	-	-	-
97	230	1.5	298	40	127	65	227	77.0	245	53.9	170	78	260
-	-	:t.	1.9	Ext.	5.4	Ext.	3.8	Ext.	3.6	Ext.	3.9	-	-
-	-	254	6.4	7.4	18.7	5.6	14.5	3.7	9.5	6.6	16.6	-	-
312	75.0	33	76.5	944	137	761	106	1005	159	-	-	-	-
59	12.0	10	43	34.8	57	252	43	340	63.5	-	-	-	-
-	-	.6	14.3	41.6	11.5	29.6	10.9	38.9	13.8	-	-	-	-
-	-	.2	2.4	1.3	3.0	-	-	-	-	2.2	5.0	5.1	10.4
14.3	9.0	.9	11.2	38.8	11.2	26.7	8.1	34.1	10.6	-	-	-	-

published by Code(12). Table III indicates that there is a systematic difference; in any event, the difference is not larger than 8 percent and consequently is not very important.

The results of the observations are presented in Table 4; both unreddened and reddened values of the line intensities are given for 11 points. In each case the intensity of H_β has been considered to be 100, absolute values can be easily obtained with the help of Table I.

D) Photographic Observations

Although the spectral resolution achieved with the scanner is enough for many problems, it is not sufficient when lines separated 10 A or less need to be resolved. Forbidden lines, useful for the determination of temperature and density, fall in this category. In addition to the spectral resolution improvement, a much higher definition of the observed areas is attained by photographic means. This higher precision is required if temperature fluctuations, as indicated by OIII line ratios, are to be determined. Changes in surface brightness over areas separated by only a few seconds of arc, can easily be seen in Figure 1. The slit of the spectrograph placed on these areas would detect changes in λ4363, and in other lines as well, with a much finer detail than the scanner observations can.

However, all of these advantages are counterbalanced by the non-linearity of the photographic plate - in addition to the well known variations of the emulsion response with the

wavelength. Smaller disadvantages like the reciprocity failure law and the intermittency effects do not introduce large uncertainties in the results since both effects can be nearly eliminated, although at the cost of very lengthy operations.

The dispersion used in the present work was nearly 85 A/mm, which permits us to resolve all the forbidden line doublets relevant to the problem; the exception being the [OII] doublet at 3727. However, in this case, multislit plates (8) at this wavelength obtained with the 200-inch telescopes, were kindly supplied by Dr. G. Münch. A description of those plates, as well as the method of reduction for obtaining the electron density will be given elsewhere.

The 4-inch camera of the Cassegrain X-spectrograph of the 60-inch telescope(23) was used in a small fraction of the program. Most of the spectrograms were obtained by means of the Newtonian B-spectrograph. This instrument was used with the 100-inch telescope and with the 60-inch as well. The 88B grating, with 15 000 lines/inch, in combination with the 3-inch Schmidt camera, gave the proper dispersion, 85 A/mm in the blue. The 100-inch telescope, having the scale of 16 seconds of arc per mm at the Newtonian focus, was used for obtaining the spectra of small condensations. Whereas the 60-inch telescope, with larger scale (27"/mm), was employed for areas containing larger condensations.

Three emulsions were needed for covering the spectral

range from 3600 to 9000 A:

a) IIaO for the region from 3600 to 5100,

b) 103aF for the region from 3840 to 6800,

c) I-N for the region from 5800 to 9000.

These last plates were hypersensitized with the well-known ammoniating process. The concentration of the NH_4OH solution was 8 percent, which gave an increase in speed of about 4, but produced plates with varying degrees of chemical fog.

A suitable and careful calibration of the photographic plate must be carried out if accurate line intensity measurements are to be made. Several standard stars were selected for this prupose as ϵ Ori, Υ Gem, 29 Psc, α Leo, which are included in Oke's list of standard stars and were observed under various conditions. Their energy distribution is accurately known and they can provide the proper λ sensitivity calibration. These stars were not trailed along the slit, but rather their image slightly out of focus was used, in this way the intermittency effect is avoided. This procedure was used notwithstanding that there might be a loss of light in both ends of the spectrogram. Since these plates were used to calibrate intervals of 300 A at the most, this problem is not important. In order to eliminate the reciprocity failure problem, a screen was used to reduce the star intensity to a certain value, which permitted exposure times nearly equal to those needed to obtain the nebular spectrum.

The calibration wedge spectrograms, needed to establish the characteristic curve of the emulsion, were also obtained with the same exposure times and developed under similar conditions. The characteristic curves were obtained by the usual tracing procedure. This process was carried out with the recording microdensitometer at the California Institute of Technology. The same instrument was used to obtain the direct line intensity measurements of both nebular and star spectrograms. The atmosphere extinction, according to Oke, can satisfactorily be represented by a slightly modified λ^{-4} law. For the photographic work the extinction was taken into account by

$$p\nu = e^{-a(\lambda) \sec z} \quad ,$$

where

$$a(\lambda) = -0.038 + 0.00862\ (1/\lambda)^4 \quad . \qquad (3)$$

The spectrogram reduction is a very lengthy process, however, the work was simplified with the use of the results obtained with the scanner observations. It can be seen from Table IV that the intensity of the HeI lines at 5876, at 4471, and at 4026, in units of H_β, is practically the same everywhere. Then, these lines can provide useful intensity standards for the spectral regions in this vicinity; characteristic curves were obtained at λ4000 and at λ4400. With these curves, the intensities of lines falling in the

intervals 200 A wide, centered at those wavelengths can be measured with respect to those standard lines with a high degree of accuracy. The intensities, measured in this way, are in units of either λ4026 or λ4471 and must still be corrected in order to eliminate the effects of the atmospheric extinction; equation 3 will give the correction value to be applied in this case, and no significant error may be introduced by this value since the wavelength interval is very small. In the same way, and with the use of the standard stars mentioned, the instrumental response variations were computed for the same wavelength regions; the correction factors were derived and found to be very small. Reciprocity failure effects are not present since the standard stars' spectrograms have nearly the same exposure times as the nebular ones. The nebular reddening was included also; the values found for the point (1) were used always, since the wavelength intervals are small no significant error is introduced with that procedure. Once the line intensities in these two regions are corrected, they can very easily be transformed to H_β units. The lines measured can in turn be used for the measurement of other nearby lines, characteristic curves must be obtained for the corresponding wavelength intervals and the same process carried out over all. Table V gives the intensity values for the lines of HeI that were measured with the process indicated. The comparison with the theoretical values (24) is also presented.

TABLE V

λ	Trans.	Theory	Observed
5876* (p	3^3D-2^3P	10	10
4471*	4^3D-2^3P	4.2	3.9
4388	5'D-2'P	0.63	0.6
4120	5^3S-2^3P	0.11	0.13
4026*	5^3D-2^3P	2.3	2.2
4009	7'D-2'D	0.24	0.20
3927	8'D-2'P	0.16	0.10
3820	6^3D-2^3P	0.12	0.18

The values shown in the table were determined from 12 spectrograms of regions where the lines 3927 and 3820 are strong enough to be measured. The agreement between theory and observations seems to be complete. The small differences present are of the same order of magnitude as the probable errors of measurement. Consequently, it was assumed that the line intensities of HeI, in the nebular spectrum, can be accurately represented by the theoretical recombination intensities. Therefore, the line intensities of the other elements can be measured with respect to a nearby HeI line of about the same intensity. The accuracy determined obviously increases when the reference HeI line is close to the line to be measured. The intensity of the important line of [OIII] at 4363, for instance, can be easily measured with respect to λ4388 with the errors being

reduced to a minimum. In addition, the intensities of the N_1 and N_2 lines can be obtained in terms of H_β (the three lines being of comparable intensity) with good accuracy. Therefore, the electron temperature that can be derived from the $4363/N_1+N_2$ ratio is also of the first order in accuracy.

The important lines of other elements were measured in the same way, although in some cases the quality of the intensity determinations is not as good as in the case of λ4363.

The results obtained with the photographic material will be presented in Chapter IV, where each individual element is considered separately.

CHAPTER III

HYDROGEN AND HELIUM NEBULAR SPECTRA

The main sources of excitation for the Orion nebula are stars of spectral type O6 and O9, namely θ^1C Ori and θ^2Ori. Consequently, the radiation field, at frequencies beyond the Lyman limit, is very strong. The radiative energy in this spectral range is absorbed inside the nebula and converted, via photoionization of the H and He atoms into kinetic energy of the stripped electrons, which by elastic collisions with each other and by inelastic with impurities (excitation of metastable levels of ions and interaction with dust particles), establish a thermal distribution of velocities. Subsequent recombination of these electrons, followed by downward radiative transitions, produce the various emission lines. It is then by this process, known as the Zanstra mechanism, that the stellar energy in the far ultraviolet, is redistributed among the H and He emission lines and can escape from the nebula.

For the hydrogen atom, the electron capture cross-sections and spontaneous transition probabilities are well determined by accurate quantum mechanical computations. Therefore, the relative intensities of the spectral lines, produced by radiative recombination, can be obtained with a great deal of precision. In computing the line intensities, some of the following simplifying assumptions have been made by various investigators.

1) The exciting star is assumed to show a spectrum with perfect black Lyman lines. That is, Lyman line radiation is produced only by the nebular process. The possibility that the excited levels are populated by stellar line radiation, is ignored.

2) Electron collisional processes do not exist.

3) There is no absorption of subordinate lines. Then, the population of excited levels is not effected by radiative transfer processes other than radiative recombination and cascade from higher levels.

4) Although collisions are not included in the physics of the problem, the orbital degeneracy of H atom is not considered. The population of the various $n\ell$ levels is given by

$$N_{n\ell} = \frac{2\ell+1}{\sum_{\ell=0}^{n-1}(2\ell+1)} N_n = \frac{2\ell+1}{n^2} N_n \qquad (1)$$

relation satisfied in thermodynamic equilibrium only.

5) If the stellar Lyman lines are included, the exciting star is assumed to radiate as a black body in the spectral region of these lines. Considering the fate of the Lyman nebular lines, some extreme cases have been considered:

Case A: The Lyman lines produced inside the nebula escape without absorption; regarding the stellar radiation, assumption 1 is made.

Case C: Same, but instead of 1, assumption 5 is taken as the working hypothesis.

Case B: Since most of the neutral atoms are in the ground

level, the nebula is optically thick in the Lyman lines. None of the nebular Lyman-line radiation, except Lyα, escapes. All other Lyman quanta being transformed, by scattering, to quanta of lower energy. Assumption 1 is made.

Computations, for an H atom with infinite number of levels with assumption 2, 3, and 4, have been carried out for cases A and B by Baker and Menzel(25) and more recently by Seaton(26). Baker and Menzel used an expression for the Gaunt factors which was not quite correct, as shown by Burgess(21); in addition, more serious numerical errors were found also by Burgess in the Case B computations. Seaton's solution corrected the errors and extended the calculations to lower temperatures.

With assumptions 2 and 3, Burgess(21) with a 12-level atom, and Searle, with a 10-level atom(27), have taken into consideration the orbital degeneracy of the hydrogen atom for Cases A and B. In addition, Burgess has introduced both a correction for the presence of the other levels and the proper expression for the Gaunt factors. Burgess' computations indicate that assumption 4 gives much better results for Case B than for Case A. The reason is simple - when 4 is assumed, the transitions to the ground state, taking place only from the np states, are overestimated.

The observations by Menon(28) clearly indicate the presence of neutral hydrogen around the nebula; therefore, the high optical thickness for the Lyman radiation is assured.

Consequently, Case B applies in those conditions. In the present work, Case B has been assumed to represent the recombination process in the nebula.

The Paschen and Balmer Lines

The recombination Balmer decrement can be affected by self-absorption and by collisional excitation as well. A comparison of the hydrogen line intensities observed, with those predicted by theory, can determine whether or not the recombination theory alone can explain the hydrogen nebular spectra. The discrepancies between theory and observations may indicate the importance played, inside the nebula, by both self-absorption and collisional excitation.

The optical depth, τ_0, at the center of Lyα, can reach high values in diffuse nebulae; the density of Ly-α quanta may be quite large since for each photoionization a Ly-α is eventually produced. Consequently, the population of the 2p level might be increased through resonance scattering, as pointed out first by Greenstein(2), and later elaborated upon by Pottasch(29). The computations of the latter author suggest that self-absorption might be important. However, that suggestion is quite objectionable on physical grounds.

If the scattering process were strictly coherent, the Lα-quantum path is merely described as a random walk process, and one can easily compute the number of scatterings as follows: Let Rn be the distance traveled by a

photon after n scattering; if k_0 is the absorption coefficient at the center of the line and N_1 the density of neutral atoms in the ground state, then neglecting extinction by dust:

$$\underline{R}_n = \underline{R}_{n-1} + \underline{i}\,(k_0 N_1)^{-1} \qquad ; \qquad \underline{i}\cdot\underline{i} = 1$$

taking the average square

$$\langle R_n^2 \rangle = \langle R_{n-1}^2 \rangle + \frac{1}{k_0^2 N_1^2} = \langle R_{n-1}^2 \rangle + \frac{1}{k_0^2 N_1^2}$$

if Q is the number of scatterings suffered before leaving the nebula, we have

$$Q = k_0^2 N_1^2 \langle R_s^2 \rangle = \tau_0^2 \qquad (2)$$

where τ_0 is the optical depth at the center of the line. The absorption coefficient at the center line, with the usual notation, is given by:

$$k_0 = \frac{\sqrt{\pi}e^2}{mc} \frac{f}{\Delta\nu_0} H(a,v) = \frac{\sqrt{\pi}e^2}{mc} \frac{f}{\Delta\nu_0} \qquad . \qquad (3)$$

When microturbulent motions of about 10 km/sec are considered, the Doppler width is, for an electron temperature of 10^4 K:

$$\Delta\nu_0 = \frac{1}{\lambda}\sqrt{\frac{2kT}{\mu H} + 10^2} = 1.35 \times 10^{11} \text{ sec}^{-1} \qquad (4)$$

then, the absorption coefficient becomes 9.3×10^{-14} cm^2/atom. Adopting 10^{18}cm as the radius of the nebula, we can see that the optical depth is of the order of 10^5. Therefore, under

the assumption of coherent scattering, each Lα photon bounces back and forth, between the 1s and 2p levels, an average value of about 10^{10} times before it can leave the nebula. This number of scatterings is extremely large, and indicates a large relative population of the 2p level of hydrogen, as can be shown with the following analysis. There are various processes which lead to the depopulation of the 2p level; the emission of a Lyα photon has the highest probability of all; therefore, the probability of absorption of a Balmer photon is small. Namely, for Hα quanta, the probability of absorption is

$$P_{H_\alpha} = \frac{I_{H_\alpha} B_{23}}{A_{21}} \qquad (5)$$

where I_{H_α} is the intensity of Hα line radiation and given by

$$I_{H_\alpha} = N_e N_{H^+} c \alpha_{32} \frac{h\nu_\alpha}{4\pi\Delta\nu} \qquad (6)$$

where α_{32} is the so-called effective recombination coefficient and $\Delta\nu$ is the width of the line. Using Seaton(26) data for the computation of α_{32}, at 10^4 K, it is found that

$$\alpha_{32} = 8.86 \times 10^{-14} \text{ cm}^3/\text{sec} \quad ,$$

and taking $\Delta\nu$ as the Doppler width

$$I_{H_\alpha} = 8.5 \times 10^{-14} N_e^2 h\nu_{H_\alpha} \quad , \qquad (7)$$

then the probability of absorption is

$$\lambda_{H\alpha} = \frac{2.015 \times 10^{-14} N_e^2}{4.68 \times 10^8} = 4.31 \times 10^{-23} N_e^2 \quad . \quad (8)$$

Consequently, the number of Hα quanta absorbed per unit volume is

$$P = Q \lambda_{H_\alpha} \text{ (number of Ly-}\alpha\text{ quanta per unit volume).}$$

Since, for Case B, the number of quanta in the Balmer lines is equal to the number of Lyman-α photons produced, we have

$$P = \lambda_{H\alpha} Q (1-X) N_e^2 \alpha_B \qquad H_\alpha\text{-photons/cm}^3 \qquad (9)$$

where α_B is the total recombination coefficient, and X, equal to 0.34, is the fraction of the electron population of the second level, which is in the state where $\ell = 0$. The energy absorbed per unit volume is

$$P h\nu_{H_\alpha} = 4\pi I_{H\alpha} N_{2p} \frac{\pi e^2}{mc} f_{2p} \quad . \quad (9b)$$

Therefore, the population of the 2p level becomes, using 9b

$$N_{2p} = 3.65 \times 10^{-22} Q N_e^2 \quad . \quad (10)$$

If, as indicated above, the scattering is coherent, with 10^5 as the optical depth in the center of Lyα, the optical nebular thickness in the center of Hα is given by

$$\tau_{H\alpha} = 3.65 \times 10^{-12} N_e^2 k_{o\,H\alpha} L \quad .$$

L is the radius of the nebular (=1/3 pc) and k_o the absorption coefficient in the center of the line. At 10^4 K, $k_{o\,H\alpha} = 3.09 \times 10^{-12} cm^2/atom$. Adopting 1500 as the average electron density of the Orion nebula (lower limit), the optical depth, at λ6563, is about 24. According to Capriotti's calculations(29), in which recombination and self-absorption are considered, the Balmer decrement obtained with that optical depth, is significantly different from the decrement predicted on the grounds of pure recombination, as seen in Table VII.

Although a comparison of the Balmer decrement observed in the present investigation with that predicted by theory would provide a sound test for the existence of self-absorption, a more direct approach to the problem can be obtained from the fact that Hα, in absorption, has never been observed in the spectra of the stars imbedded in diffuse nebulae (30). From this clear evidence one can directly derive the population in the 2p level and compare it with the values derived above.

If it is assumed that the minimum detectable line has an equivalent width of 0.01, using the curve of growth

(Unsold's book, page 292), one obtains the value for the abscissa

$$\log \frac{N f}{\Delta \omega_0} = -0.50$$

With $f_{2p} = 0.71$, one obtains the condition

$$N_{2p} L \leq 7 \times 10^{10}$$

$$\therefore \tau_{2p} \leq 0.22 \qquad (11)$$

On the other hand, from equation 10, in general:

$$N_{2p} L = 3.65 \times 10^{-22} \varphi N_e^2 L \qquad (12)$$

with the values adopted before

$$N_{2p} L = 8.24 \times 10^{12} ,$$

which is two orders of magnitude larger than what the condition(11) imposes, as a maximum value.

Since the arithmetic carried out above involves atomic constants and well-determined quantities only, the result obtained clearly indicates that the assumption of coherent scattering is not sound. Furthermore, the existence of significant self-absorption of the Balmer lines can be ruled out for the case of the Orion nebula.

Osterbrock(27), using an approximate diffusion theory, has considered the case when the scattering of the Ly-α photon is not a coherent process. He has con-

sidered the general case when there is a correlation between the frequencies of the Ly-α quanta before and after scattering. The formula for the redistribution in frequency of a photon after scattering, as a function of its frequency before it has been scattered, has been derived by Unno(32), and used in Osterbrock's analysis. His results indicate that for a nebula with $\tau o_{L\alpha} = 10^5$, an average photon is scattered about 8×10^5 times; whereas, for a nebula with $\tau o_{L\alpha} = 10^6$, Q becomes close to 10^7. Therefore, one obtains, for the case of the Orion nebula, through equation 12, when dust effects are neglected too,

$$N_{2p} L = 6.7 \times 10^9$$

$$\tau_{2p} \simeq 0.02$$

result which is in excellent agreement with condition 11, as set by direct observations. However, as can be computed for planetary nebula where the density is of the order of 40 000 cm^{-3} and τo close to 10^6, the optical depth for Hα becomes close to 10, and as a consequence, for those planetary nebula, the possibility of self-absorption still remains an open question.

The effect of self-absorption of the Balmer lines would increase the strength of the nebular Hα, H_β, HY over the recombination value, since every time a Balmer line is absorbed, the electron in an excited level, higher than n = 3, cascades down either by the emission of the same line or by the emission of two lines of lower energy, namely, the absorption of an H_β photon would produce a Paschen-α

photon plus an H-α photon; the absorption of an HΥ line would create one of the following combinations: Hα plus Pβ; Brackett α, Pα, and Hα; Hβ plus Brackett α. That is, the energy of the higher member of the Balmer lines is transferred, by self-absorption, to the lower member plus the emission of lines of other series. Therefore, the effects of self-absorption will show up more clearly in Hα, Hβ, and HΥ than in any other line.

If, notwithstanding the low electron density, collisional excitation occurred in the nebula at a temperature of about 10 000 K, the lines would be enhanced accordingly to the excitation potential of the upper levels, from which the lines arise; the higher the potential, the weaker the line produced. As pointed out by Chamberlain(33), collisions begin to be effective in populating the excited levels only when the electron temperature is higher than 1.5×10^{40} K. However, Chamberlain's arguments are based on the hypothesis that collisions take place with atoms in the ground state only, the possibility of collisions with atoms in the 2p level, has not been considered.

If self-absorption occurs, in addition to the radiative recombination, then:

$$\log (H\beta/H\Upsilon) > \log (H\beta/H\Upsilon)_{\text{recombination}} = 0.31$$

$$\log (H\alpha/H\beta) > 0.42 \quad .$$

If both processes, collisional excitation and self-absorption, were working simultaneously, the effects in the HΥ/Hβ ratio

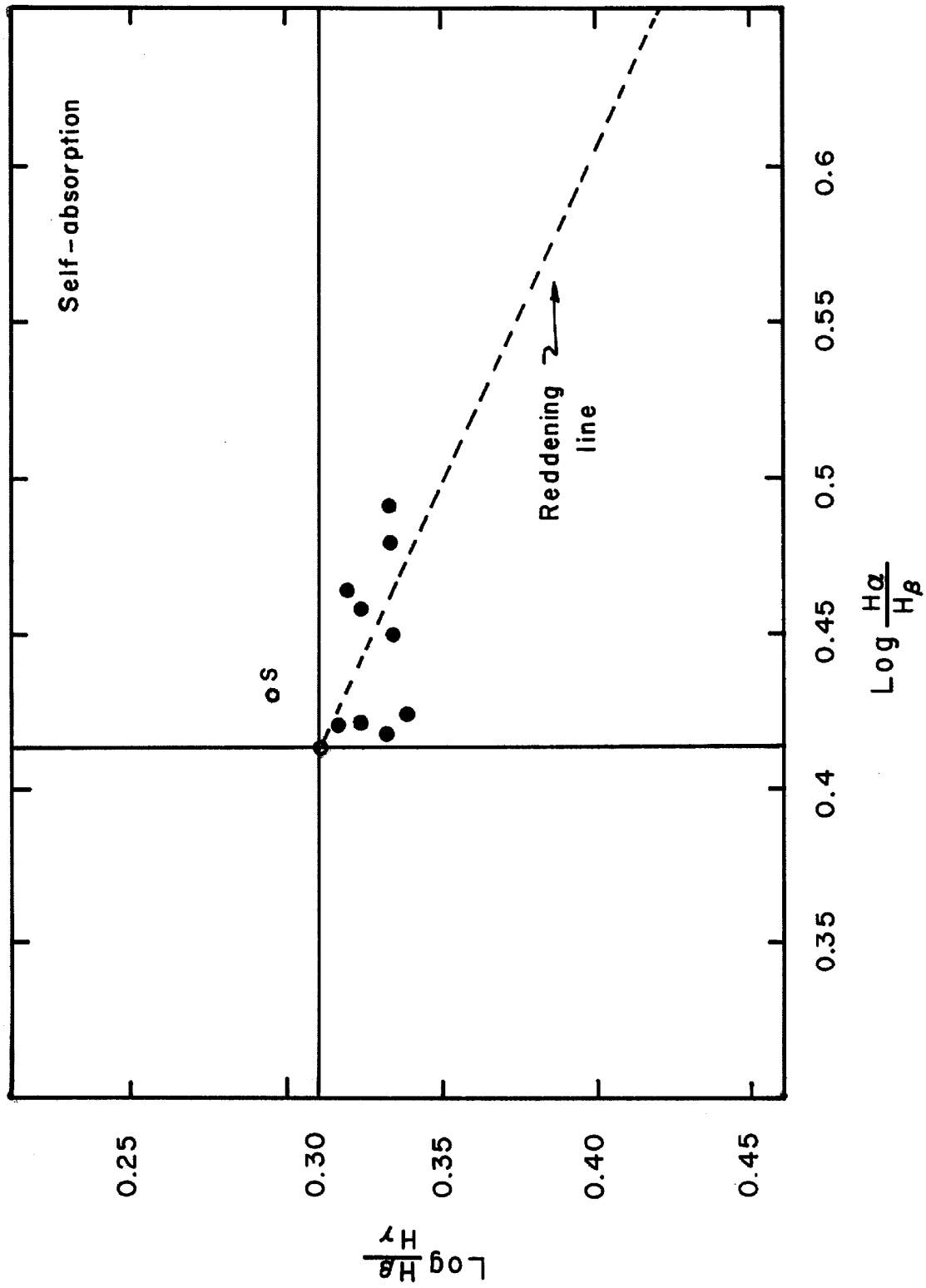
Self-absorption
Reddening line
2
os
0.25
0.30
0.35
0.40
0.45
0.35
0.4
0.45
0.5
0.55
0.6
$\log \frac{H\beta}{H\gamma}$
$\log \frac{H\alpha}{H\beta}$

would tend to cancel out, whereas the strength of Hα would always be increased.

The logarithms of the corresponding ratios, found in this investigation, are given in Table VI and plotted graphically in Figure 3 (filled circles). The theoretical recombination values as given by Burgess(21) and b Seaton(26) are represented by the open circles.

TABLE VI

Point	log H_α/H_β	log H_β/H_α
1	0.43	0.325
2	0.43	0.315
3	0.412	0.335
4	0.47	0.325
5	0.49:	0.34
6	0.45	0.33
7	0.416	0.34
8	0.48	0.335
9	0.46	0.32

It can be seen that all the points are close to the theoretical recombination values, but do not agree with them. The average for the log Hβ/HΥ is higher, by 0.022, than the theoretical prediction; whereas the average of log Hα/Hβ is also higher by about 0.032. The same discrepancy, in the same direction, of the Hβ/HΥ ratio, has been found by Mathis(20), who also has observed the Orion nebula using a photoelectric scanner; although the discrepancy

found here is half of that indicated by Mathis, probably due to differences in the reddening correction. Moreover, Osterbrock et al(34), after the photoelectric observations of relative fluxes in Hα, Hβ, and HΥ of ten planetary nebula, suggest the possibility of a calibration error of about 0.04, at HΥ. As for the case of the Hα/Hβ ratio, the discrepancy is of the order of 8 percent, which is far too high to be explained in terms of measuring errors, which for this strong line are not larger than 3.5 percent. The influence of the λ6548 of NII cannot account for more than 2 percent. Consequently, on the average, there is a discrepancy of the order of 5 percent with respect to the recombination value as predicted by Burgess' computations, but only of 3 percent with respect to the decrement as computed by Seaton.

If the possibility of the calibration error at HΥ were not accepted, the overall position of the points would indicate the existence of significant collisional excitation affecting the recombination Balmer increment. From Chamberlain's(33) results, such a possibility can be ruled out (if only collisions with neutral hydrogen in the ground state are considered). Therefore, on the basis of the similarity of the results presented here, with those of Osterbrock et al and Mathis, it is concluded that the HΥ/Hβ ratio discrepancy can be explained in terms of a small error in the calibration; however, the Hα/Hβ ratio is larger, by about 5 percent, than the expected theoretical value. A possible explanation for the latter discrepancy can be advanced by noticing that all

the points showing larger Hα/Hβ ratios lie farther from the center than the points with smaller ratios. If the reddening curve developed a small curvature close to the Hα wavelength when the points are far from the center, smaller absorption values may be derived by the use of the lower shape shown in Figure 1. However, the possibility of that discrepancy in the Hα/Hβ ratio being real still remains.

Since the discrepancies of the Hα/Hβ and Hγ/Hβ ratios with respect to the theoretical recombination are relatively small, one can expect still smaller differences for the other lines. Table VII shows the comparison of the observations with the theoretical values given by both Seaton and Burgess for the pure recombination Case B; Burgess' values, with the orbital degeneracy included, are in brackets. Capriotti's calculations, allowing for self-absorption of the Balmer lines where the optical depth in Hα is 25, are also given (35).

TABLE VII

Line	Pure Recombination (T_e = 10 000 K)	Self-Absorption τ_α = 25 (T_e = 10 000 K)	Point (1) Observed Ratios
10938	(9.8)	11.6	10.0
10049	(6.5)	7.4	6.0
9229	(3.3)	4.1	3.3
8862	(2.5)	2.4	1.1:
6562	271(262)	347	265
4861	100	100	100
4340	50.6(48.9)	55.1	47.2
4101	29.8(27.6)	32.6	29.0
3970	19.2(17.2)	20.7	blended
3889	13.2(11.2)	13.8	blended
3835	9.5	11.6	9.3
3798	7.2	8.7	6.6
3770	5.4	6.6	5.5 pg.
3750	4.2	5.2	3.7 pg.

The values obtained from point 1 observations are shown in Table VII; but, as can be seen from Table IV, almost the same values are obtained for the other points. The lines λ3770 and λ3750, with principal quantum numbers 11 and 12, respectively, were measured photographically; in this way, the continuum can be accurately taken into account. With the lower resolution of the scanner, the intensities of these lines were found to be about 40 percent smaller. The Paschen line, at λ8862, seems to be seriously affected by the molecular

absorption of the earth's atmosphere.

According to the data of Table VII, the agreement between the recombination values and the observations is very good. Notwithstanding the small discrepancies in Hα, it can be concluded that the hydrogen nebular spectra is predominantly produced by pure recombination processes. This close agreement provides a check, not only on the validity of the theory, but also on the assumption made that Case B holds in the nebula.

Helium Spectra and the He/H Ratio

1) The 2^3S Level

From the results obtained for the hydrogen emission spectra, one might expect that recombination alone can also explain the helium nebular spectra. As in the case of hydrogen, the radiative transitions are so large, compared with the time between collisions, that the various levels are populated by either direct recombination or by downward cascades. However, in the case of helium, some upper triplet levels may be populated by transitions from the 2^3S metastable level. The mean lifetime of the level, t_{2^3s}, is given by the reciprocal of the depopulation rate

$$t_{2^3S} = \left(A + \beta N_e + \gamma \nu^{-2}\right)^{-1} \quad \text{sec.} \qquad (13)$$

where A, equal to $2.2 \times 10^{-5} \text{sec}^{-1}$, is the transition probability of decay to the ground level by two-photon

emission (36), f is $\langle \sigma v_e \rangle$, the depopulation rate by electron collisions, close to 10^{-8} as estimated by Münch and Wilson(6). The probability of photoionization by the exciting star, P, at the distance, r, is $1.7 \times 10^{-6} sec^{-1} pc^2$ for the Orion nebula(6,7). With the quantities adopted before, the mean lifetime is about 1.9×10^4 sec, five orders of magnitude longer than the corresponding value of the 2^2S level of hydrogen (about 0.11 sec), for the same conditions. However, such a long lived level produces effects that are not compatible with the observations, as one can see from the following analysis.

The population of the 2^3S level is given by

$$N(2^3S) = N_e \, N(He^+) \, \alpha(\text{triplets}) \, t_{2^3S} \qquad (14a)$$

where α(triplets) is the effective recombination coefficient, quantity which has been computed by Burgess and Seaton(37), with a fair degree of precision; for Te = 10^4 K, its value is 20.97×10^{-14}. As is shown in a later part of this chapter, for the Orion nebula we have:

$$N(He^+) = 0.091 \, N_{H^+}$$

with the numerical values indicated:

$$N(2^3S) = 3.66 \times 10^{-10} \, N_e^2 \qquad (14b)$$

There are two helium lines in the spectral range

covered by our observations, with the 2^3S metastable state as lower level; namely they are λ10839 and λ3889. An over-population of the level would necessarily lead to self-absorption of those lines. However, the absorption of the λ10830 quanta would not be appreciable, simply because the radiation at this wavelength, once absorbed, is immediately reemitted ($A2^3P-2^3S=1.1 \times 10^7 sec^{-1}$). But, when a λ3889 photon is absorbed, the 2^3S state electron is now excited to the 3^3P level, from where it can either decay to the 2^3S level again or by the emission of a λ42,955 photon decay to the 3^3S level. From this level the electron must decay to the 2^3P level, with the consequent emission of a λ7065 quantum. Finally, through the transition to the 2^3S state, a photon at λ10830 is produced. Thus, with the second alternative, a λ3889 is degraded into three photons of lower energy. To be specific, by self-absorption a fraction of the λ3889 quanta, produced by recombination, are converted into photons of lower energy. The net effect being a decrease of the λ3889 intensity as the optical depth in that line increases.

2) The λ3889 Line

The optical depth, at the center of that line is

$$\tau_o(3889) = 3.66 \times 10^{-10} N_e^2 R_o L \qquad (15)$$

with $k_o = 6.2 \times 10^{-14} cm^2$ and $L = 10^{18} cm$, the optical depth is $2.21 \times 10^{-5} N_e^2$. For the central part of Orion, where N_e^2 (unreddened) is of the order of 3×10^7 (as will be shown later), the optical depth at λ3888 is of the order of 700. Such a high value would certainly lead to the complete absorption of that line and consequently no emission at that wavelength would be observed at all. In fact, for that extreme case, the whole set of triplet lines, as produced by recombination, would be effected sufficiently to be detected observationally. Table VIII gives the comparison of the intensities of the triplet lines observed with those predicted by theory.

The recombination intensity values were computed using the recombination coefficients published by Burgess and Seaton (37), for $\ell = 0$ and $\ell = 1$. For the cases $\ell \geq 2$, the helium terms become very nearly hydrogen-like, simply because the 1s electron forms a spherically symmetrical cloud of negative charge around the nucleus. For the outer electron, the field outside this cloud will be roughly identical with a field due to a single charge e at the origin. The recombination coefficients, with the hydrogenic approximation, are then (37):

$$\alpha(He, n^1L) = \tfrac{1}{4}\alpha(H, nL)$$
$$\alpha(He, n^3L) = \tfrac{3}{4}\alpha(H, nL) \quad . \qquad (16)$$

The self-absorption data came from Pottasch's computations(38). That author considered a 14-level atom and determined the relative intensities of some lines in the triplet system as a function of the optical depth in λ3889. The highest value of the latter quantity considered by Pottasch being 30. The line intensities for $\tau = 700$ have been crudely extrapolated from his results.

TABLE VIII

Line	Transition	Recom-bination	Self-Absorption		Point 1	Point 3
			τ=10	τ=700:	$I(H_\beta) = 100$	
10830	2^3P-2^3S	16.0	18.4	21.0:	43.0	60.8
7065	3^3S-2^3P	1.9	6.7	9.2	6.6	6.0
5876	3^3D-2^3P	10.0	10.0	10.0	10.0	11.1
4471	4^3D-2^3P	4.2	3.9	3.8	3.9	4.3
4026	5^3D-2^3P	2.3	1.9	1.7	2.2	2.9
3889	3^3P-2^3S	10.8	3.3	<<0.1	2.8	4.8

The intensity of the emission line λ3889, which is blended with H_8, can be obtained by assuming that the intensity of the hydrogen line is 13.2, as given by the recombination theory.

According to the table, the intensity of the lines observed, sensitive to optical depth, are markedly different from the corresponding recombination values. However, if one compares with the results obtained by Pottasch, the optical depth, at λ3889, is at least two orders of magnitude smaller

than that which was computed with Equation 15. The value of the optical depth, as suggested by Pottasch' computations, lies marginally between 8 and 10.

A direct estimate of the optical depth, at the λ3889 helium line, can be obtained by the strength of this line, which is shown in absorption in the spectra of some of the stars imbedded in the nebula(39). The equivalent widths observed in the spectra of the Trapezium stars are close to 0.2A. From the curve of the growth, for both pure thermal Doppler broadening and 10 km/sec turbulent motions, it is found that for

$$\frac{W_\lambda}{2\Delta\lambda_0} = 0.63$$

the number of atoms in the 2^3S level is

$$L\, N(2^3S) = 3.72 \times 10^{13} \quad . \qquad (17)$$

With the value of the absorption coefficient given above, the optical depth is about 3. This value is not very different from that derived using the emission line observations. Therefore, the population of the metastable 2^3S level, as predicted by Equation 14a is larger, by at least a factor of 100, than the population indicated by direct observations.

In order to explain this disagreement between theory and observations, Würm(7) has proposed a radical change in the spatial arrangement of the gas and the stars in the Orion nebula. He proposes that the exciting star

lies in front of the bright material, whereas only a cloud of lower density, where the λ3889 absorption line is produced, is in front of the star. Therefore, he assumes that the density in that cloud is such that Equation 14b leads to the same value of $N(2^3S)L$ given in 17. Consequently, under Würm's assumptions, Ne^2 must be one-hundred times smaller than the unreddened 3×10^7 introduced above. The surface brightness of the cloud, lying in front of the star, is then 100 times smaller too.

A more reasonable explanation for that discrepancy has been advanced by Münch(9), namely that the lifetime of the 2^3S level has been overestimated. He has pointed out that the effects of the Ly-α quanta have been completely ignored. In fact, a Ly-α photon has enough energy to ionize the HeI atom from the 2^3S level. In order to prove the importance of this mechanism in depopulating that metastable level, the rate of ionization by this process must be estimated, and then compared with the other depopulation rates. The analysis presented here is different from that given by Münch. Although more simplified, the treatment of the problem as shown below, avoids the introduction of the stellar parameters: effective temperature, ratios, distribution of energy, etc. involved in the arguments used by Münch.

The intensity of Ly-α radiation over the face of the nebula is given by:

$$I(L_{y-\alpha}) = \frac{\alpha_B}{4\pi}(1-X) \quad L N_e^2 \quad ,$$

the units being photons cm^{-2} sec^{-1} $steradian^{-1}$. Therefore, the ionization rate is

$$n_a = 4\pi I(L_{y-a})\, a_\nu\, Q \qquad (18)$$

where a_ν is the continuous absorption coefficient from this level. Using Su Shu Huang(40) computations, it is seen by linear interpolation that

$$a_\nu = 1.52 \times 10^{-18} \quad cm^2$$

Introducing the numerical values used above, the rate is:

$$n_a = 2.51 \times 10^{-31}\, Q\, N_e^2\, L \qquad (19)$$

From the arguments presented in the last section, Q, the number of Ly-a scatterings, is of the order of 8×10^5, as estimated by Osterbrock. Ne^2L can be derived directly from the surface brightness; however, the extinction of dust inside the nebula must be taken into consideration. As computed in a latter section, this quantity is close to $10^{25.52}$ cm^{-5}. From these values, it can be easily seen that the ionization rate is of the order of unity. This high ionization rate indicates a much more effective depopulating process than any of the mechanisms considered in Equation 13. This result should be expected. The density of Ly-a photon is very high inside the nebula, overcoming the small ionization

cross-section of the 2^3S level for radiation at the wavelength of the Ly-α line.

From Equation 14a, the population of the level is (since n_α is the only important term),

$$N(2^3S) = 0.09\, N_e^2\, \alpha(\text{triplets})\, n_\alpha^{-1}$$

using Equation 19,

$$N(2^3S) = 7.61 \times 10^{18}\, (QL)^{-1} \qquad (20)$$

the optical depth, at the center of λ3889 is, for Te = 10^4 K,

$$\tau_o(3889) = 4.72 \times 10^3\, Q^{-1} \qquad (21)$$

If as above, Q is taken as 8 x 10^5, value corresponding to an optical depth of 10^5 at the center of Ly-α, $\tau(3889) = 0.006$. This quantity is about 330 times smaller than the optical depth indicated by the strength of the λ3889 line. However, this discrepancy can be explained in terms of extinction by dust particles. Ly-α radiation is certainly absorbed by dust; then reducing the number of photoionization rate from the 2^3S level. Therefore, in the central regions, where the Ly-α quanta density is high, the optical depth at λ3889 is very small. Those regions producing the HeI lines according to the recombination theory. Whereas, in the regions farther apart from the exciting star, where the number of Ly-α quanta available for photoionization is drastically reduced due to extinction by dust, the

departures from the recombination theory occur, here the lifetime of the 2^3S level is longer. The optical depth, at λ3889, becomes close to unity and the self-absorption effects come into operation. It is in these outer regions where that line, shown in absorption in the spectra of some stars, is formed.

This assumption on the stratification in the line formation mechanisms, can be supported by the radial velocities derived from the nebular He absorption lines. Table IX merely reproduces part of the data already presented by Würm(7). That table gives the radial velocity of the nebular gases, as determined by both the nebular emission lines and the helium absorption lines. The emission line data comes from the work of Wilson et al(8). The velocities from the HeI absorption lines were determined by Wilson(9). It can clearly be noticed that the HeI always indicate a higher velocity of approach, toward us, than the emission nebular lines do.

TABLE IX

Star	(OIII) Lines	(OII) Line	H_γ	He λ3889
P1865 θ^1Ori A	+17.0	+20.9	+17.0	+5.0
P1863 θ^1Ori B	+19.0	+20.0	+19.0	-6.0
P1891 θ^1Ori C	+25.0	+23.0	+22.0	+4.0
P1993 θ^2Ori	+14.0	+16.0	+14.0	+2.5
P2031 θ^2Ori faint	+9.1	-	-	+4.5

The fainter components of the HeI lines have been omitted from the table, as well as the splitting in the (OIII) lines; this emission does not alter that correlation significantly. If only the 4 Trapezium stars are considered, it can be concluded that a difference in velocity of about 18 km/sec, on the average, exists between the outer regions where the HeI is formed and where the inner zones bright emission lines are produced. This gradient of velocities is in agreement with the assumption that the nebular is expanding and that there is a stratification in the HeI line formation mechanisms.

3) The λ10 830 Line

It can be noticed from Table VIII that the intensity of this line is markedly different from that predicted by the recombination theory. Furthermore, the strength of the line

is even greater than the value predicted with the extreme cases of self-absorption. This discrepancy exists because electron collisional effects have been wholly neglected. Since the energy difference between the 2^3S and 2^3P levels is small, the collision effects are bound to become important in the outer regions, where the population of the 2^3S level can be high. The collisional deexcitation rate from the 2^3P level is negligible compared with the spontaneous optical transition rate to the 2^3S level (emission of λ10 830); therefore, any number of upward collisional transitions to the 2^3P level would lead to the emission of the same number of λ10 830 quanta.

The number of λ10 830 photons produced, per unit area per second, due to electron collisions is:

$$P(10\,830) = L\, N(2^3S)\, N_e \langle q v_e \rangle \qquad (25)$$

where $\langle q v_e \rangle$ Ne gives the upward collisional rate. From the work of Seaton(41), at 10^4 K:

$$P(10\,830) = 2.8 \times 10^{-7}\, N(2^3S)\, N_e$$

The number of photons P can be obtained through the use of Tables I, IV, and VIII. Table I gives the surface brightness at Hβ for all the points observed in Rayleigh's (10^6 photons/$cm^{-2}sec^{-1}$). From Table IV, the I(10 830)/ $I(H_\beta)$ ratio is obtained. Interpolation in Table VIII,

using the intensity of either λ3889 or λ7065, provides both the optical depth at λ3889 and the fraction of the λ10 830 photons produced by electron collisions. For point 1, the surface brightness is 102 x 10^3 Rayleighs, the I(10 830)/ $I(H_\beta)$ ratio is 0.43. Judging by the intensities of both λ3889 and λ7065, the optical depth at λ3889 is about 9. Consequently, since $I(5876)/I(H_\beta)$ is nearly 10, the fraction of λ10 830 quanta induced by collisional excitation is:

$$\frac{43.0 - 18.4}{43.0} = 0.57$$

then, taking into account that

$$\frac{h\nu(H_\beta)}{h\nu(10\,830)} = 2.22$$

P is given by

$$P(10830) = 2.22 \times 0.43 \times 102 \times 10^9 \times 0.57$$
$$P(10830) = 5.6 \times 10^{10}$$

Using Equation 25 with an adopted value of Ne = 750, for the outer regions, one obtains

$$N(2^3S)\,L = 2.7 \times 10^{14}$$

If this number is multiplied by the absorption coefficient at the center of λ3889, we have

$$\tau(3889) = 16.8$$

This value is nearly a factor of 2 greater than Pottasch computations suggest for this point ($\tau = 9$). It must be pointed out that there is still an extinction correction

to be applied; the amount of radiation lost by dust absorption at λ10 830. This effect would still increase the optical depth; if one adopts the reddening curve as drawn in Figure 2, the correction is about 0.3 mag. The optical depth would then be 22.1. However, that correction would be correct only if the dust, producing the nebular extinction, is located at the edge of the nebula. But, if that were the case, the relatively small reddening indicated by θ^2Ori, as compared with the large extinction shown by the Trapezium stars, would be difficult to explain. Consequently, the idea that dust is mostly distributed in regions close to the center is preferred. Therefore, the reddening correction must be much smaller and can be safely ignored.

In any event, the optical depth at the center of HeI λ3889, as derived with the intensity of the λ10 830 emission line, is much smaller than that obtained when the mean lifetime of the 2^3S level is considered to be given by Equation 13 only. That is, the intensity of this strong emission line is also consequent with the hypothesis, given above, that the Ly-α quanta play the dominant role in the depopulation of the level.

The departures from the recombination values are greater in λ10 830 than in any other line within the triplet system. Those departures are mostly due to collisional effects. The efficiency of the electron collisions is directly proportional to the population of the 2^3S level, which in

turn depends on Q , the average number of scatterings suffered by Ly-α photon before leaving the nebula. Let m be the ratio of the upward collisional transitions (to the 2^3P level) to the rate of λ10 830 produced by recombination, then

$$m = cte' \cdot \frac{N(2^3S)\, N_e \langle Q V \rangle}{N(H_o^+)\, N_e\, \alpha_{2p,2s}} \qquad (26$$

where $\alpha_{2p,2s}$ is the effective recombination coefficient at Te = 10^4 K. From Equation 20, and using $N(He^4) \approx 0.090$ Ne, m becomes:

$$m = cte \cdot \frac{1}{N_e Q L} \qquad . (27)$$

As indicated above, Q must be decreased due to Ly-α extinction produced by the nebular dust grains; if Qo is the number of scatterings of a Ly-α quantum in a dust-free nebula (as given by Osterbrock), then as an approximation

$$m = cte \quad \frac{\exp\left[\int_o^l \rho_o k_\lambda ds\right]}{N_e Q_o L} \qquad (28)$$

where ρ_o is the mass density of solid particles and k_λ is the corresponding absorption coefficient at λ1216. According to Equation 28, there should be a correlation between the intensity of the λ10 830 emission line and the amount of dust. The line is expected then to become stronger either for points far away from ionization sources (hot stars) or for regions with a large concentration of dust. Figure 4 shows the ratio m, for all the points where the line was observed, against

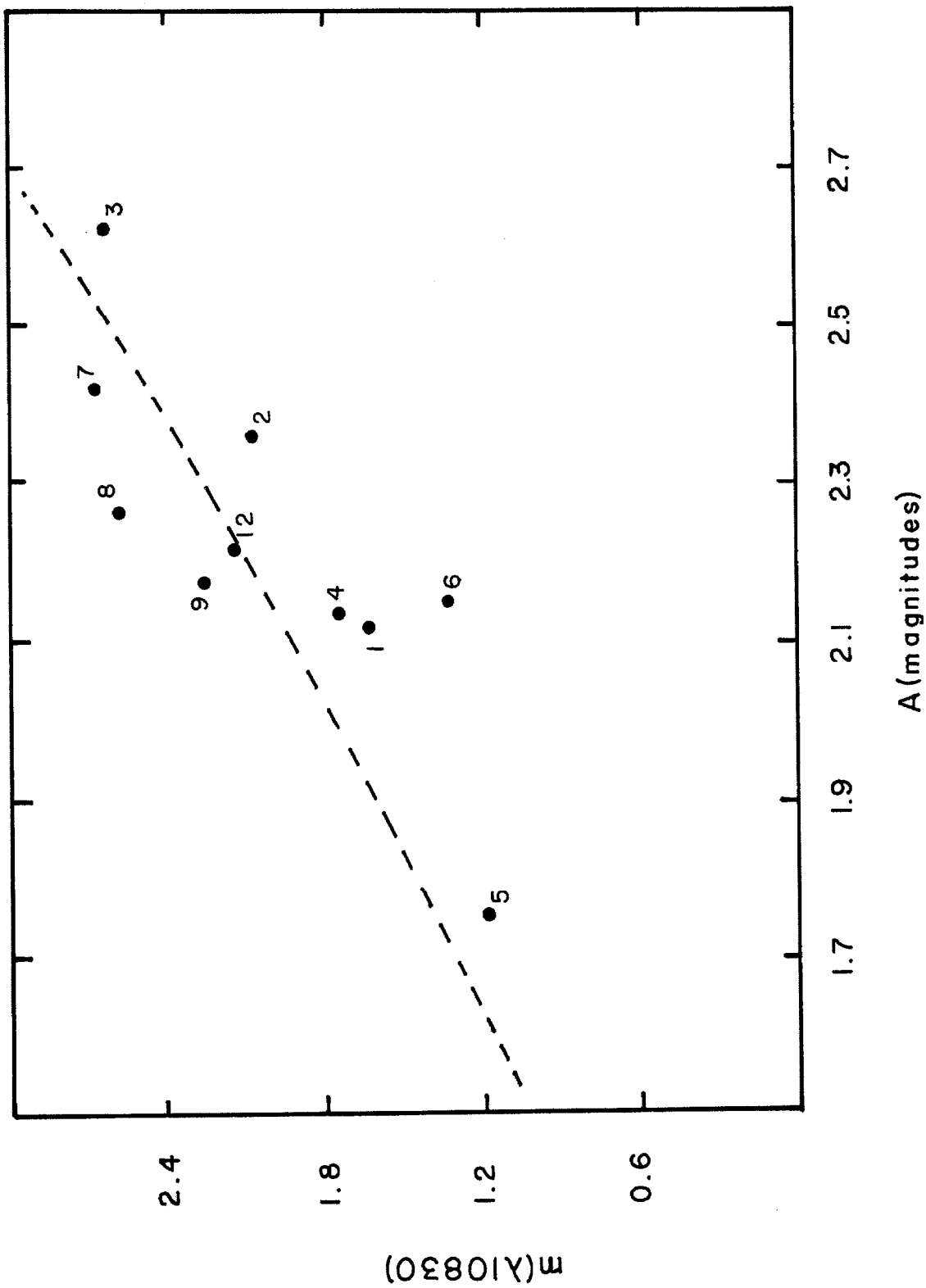

Figure 4

the "absorption" at Hβ. The value of this absorption, $A_{H\beta}$, is the differential extinction between λ10 938 and λ4861, as derived from the Paschen/Balmer ratio method.

The correlation between m and the extinction seems to be firmly established, according to the points plotted in Figure 4. However, although the ratio is almost inversely proportional to the electron density. The correlation of m with Ne does not appear very clear at first sight. The reason being the electron density fluctuations present in the outer regions, where the electron collisions enhance the λ10 830 line over the recombination value and according to the foregoing discussion. The presence of those fluctuations in electron density was clearly demonstrated by Osterbrock(5), through [3727]-line observations. The character of those variations in density were further investigated by Pariiskii(42), who found that the density fluctuations grow with distance from the Trapezium stars. Moreover, the observations of Ne provide information heavily weighted by the inner regions and consequently, the electron density of Equation 28 is not the same as the one derived throughout the surface brightness measurements. A direct photograph at λ10 830 - now quite feasible through image-tube techniques - should provide additional support for the stratification of HeI line formation mechanisms proposed in this investigation.

4) The He/H Ratio

In the previous sections, the contribution of the

line formation mechanisms, other than pure radiative recombination, has been considered. It was then concluded that, for the H spectra, the relative intensities of the various emission lines are accurately described by the recombination theory. For the case of He, some small effects, due to self-absorption, must be taken into account in addition to the recombination theoretical predictions.

The He/H abundance ratio can be determined by the line intensity ratio of HeI λ5876 and HλΔ861. The emission line λ5876 is a member of the triplet system, which is effected by self-absorption. Throughout the latter process, photons of higher energy, namely λ3889 quanta, are degraded to photons of lower energy, which include a small fraction of λ5876 photons. Therefore, the net effect of self-absorption is to increase the intensity of λ5876 over the pure recombination value. For point 1 (the best one observed), the optical depth at λ3889 is about 10. Pottasch' computations(38) indicate an increase of about 5 percent in the intensity of λ5876 for that optical depth, due to self-absorption. For the same point, the 5876/Hβ ratio is 0.098, that is, 0.0935 due to pure recombination. From the recombination coefficients as given by Burgess, one derives

$$\frac{N(He^+)}{N(H^+)} = 0.98 \frac{I(\lambda 5876)}{I(\lambda 4861)} \qquad (29)$$

and also

$$\frac{N(He^+)}{N(H^+)} = 2.41 \frac{I(\lambda 4471)}{I(\lambda 4861)}$$

If the ratios given for point (1) (which are close to the average of all) are adopted as the representative values for the whole nebula, the abundance ratio is:

$$\frac{N(He)}{N(H)} = 0.091 \pm 0.004$$

The ratio H/He, of 11 to 1, found in this work can be compared with similar determinations for other diffuse nebulae. Mathis(20) has revised his older spectrophotometry (1) for the Orion nebula given a smaller ratio - 8.5 to 1, however, his reddened values for the 5876/Hβ ratio, from which the abundance is derived, are almost equal to the ratios observed in this work. As has been pointed out before, the Paschen/Balmer ratio method indicates a larger reddening than the extinction obtained by the six-color photometry of the Trapezium stars. Consequently, Mathis unreddened value of the 5876/Hβ ratio is larger, by about 20 percent, than the value given here. He also has observed three other diffuse nebulae, one of them (NGC 604) extragalactic, in M33; in his work, the Whitford law of reddening was used to determine the corresponding nebular extinction. However, dust, inside diffuse nebulae, seems to show different behavior than in the ordinary interstellar space. Therefore, the reddening law found in Orion was employed here to correct Mathis' observations. Table X gives the results for other objects similarly studied.

TABLE X

Nebulae	He/H	References
NGC 1976	11 to 1	
NGC 6523	11.8	Mathis (20)
NGC 6514	12.4	"
NGC 604	9.7	"
NGC 2070	13.1	Faulkner (43)
NGC 346	11.0*	Aller and Faulkner (44)
IC 418	9.4	O'Dell (45)

*Ratio corrected with better b factors

Considering that errors of about 10 percent were involved in those determinations, it is clearly seen that the He/H ratio is very uniform among those nebulae. The abundance derived, from the observations obtained here, is in very close agreement with the average value of 11.4 for the six other diffuse nebulae.

5) The Dust Inside the Nebula

A direct estimate of the amount of dust imbedded in the nebula can be provided by radio observations, which are not affected by the existence of dust inside the nebula. Free-free transitions produced by electrons, in the electric field of ions, are the source of radio emission. As is well known, at wavelengths smaller than 10 cm, the diffuse nebulae are optically thin; the thermal radio intensity is

then proportional to the emission measure, and consequently can be directly related to the optical line-intensity in the following manner:

The energy flux at H_β is, at the face of the nebula

$$\mathcal{F}_\beta = N_e^2 \alpha_{4,2} h\nu_{4861} L ,$$

while the same quantity, per unit frequency interval, in the radio region is

$$\mathcal{F}_\nu = 4\pi K_\nu B_\nu L = \frac{8\pi k_\nu T_e \nu^2}{c^2} L \qquad (30)$$

where the volume absorption coefficient K_ν is, according to Smerd and Westfold (54):

$$K_\nu = \frac{4 N_e N_i Z^2 e^6}{3\left[2\pi (mkT)^3\right]^{1/2} c\nu^2} \ln\left(1+\nu_0^2\right) , \qquad (31)$$

The ratio is then:

$$\frac{F_{\lambda<10\,cm}}{F_{H\beta}} = 1.69 \times 10^{-13} \frac{\ln\left(1+\nu_0^2\right)}{T_e^{1/2}} , \qquad (32)$$

where now F gives the power received at the earth. The logarithmic factor, for the cm region, is given by:

$$\ln\left(1+\nu_0^2\right) = \ln\left[1 + \left(\frac{60}{32}\frac{(kT)^{3/2}}{ce^2}\left(\frac{2}{m\pi}\right)^{1/2}\lambda\right)^2\right]$$

TABLE XI

Point	Unreddened $F(H_\beta) \times 10^{-10}$ erg/cm^2/sec	Distance (sec. of arc)
1	13.0	45
2	9.7	68
3	12.0	32
4	9.2	104
5	0.5	151
6	4.0	105
7	6.3	87
8	3.4	100
9	2.1	115
10	11.5	55
11	4.8	120
12	8.1	80
14	0.1:	185
R	4.0	125

For a wavelength of 3.15 cm and $T_e = 10^4$ K, the logarithmic factor is 20.9, and then the relation follows

$$F_{H_\beta} = 2.8 \times 10^{13} F_{3.15}$$

The energy flux received at the earth can be obtained directly from the surface brightness data of Table 1. Those values must be multiplied by the solid angle subtended at the telescope by the entrance aperture as projected on the nebula. The distribution of the energy

Figure 5

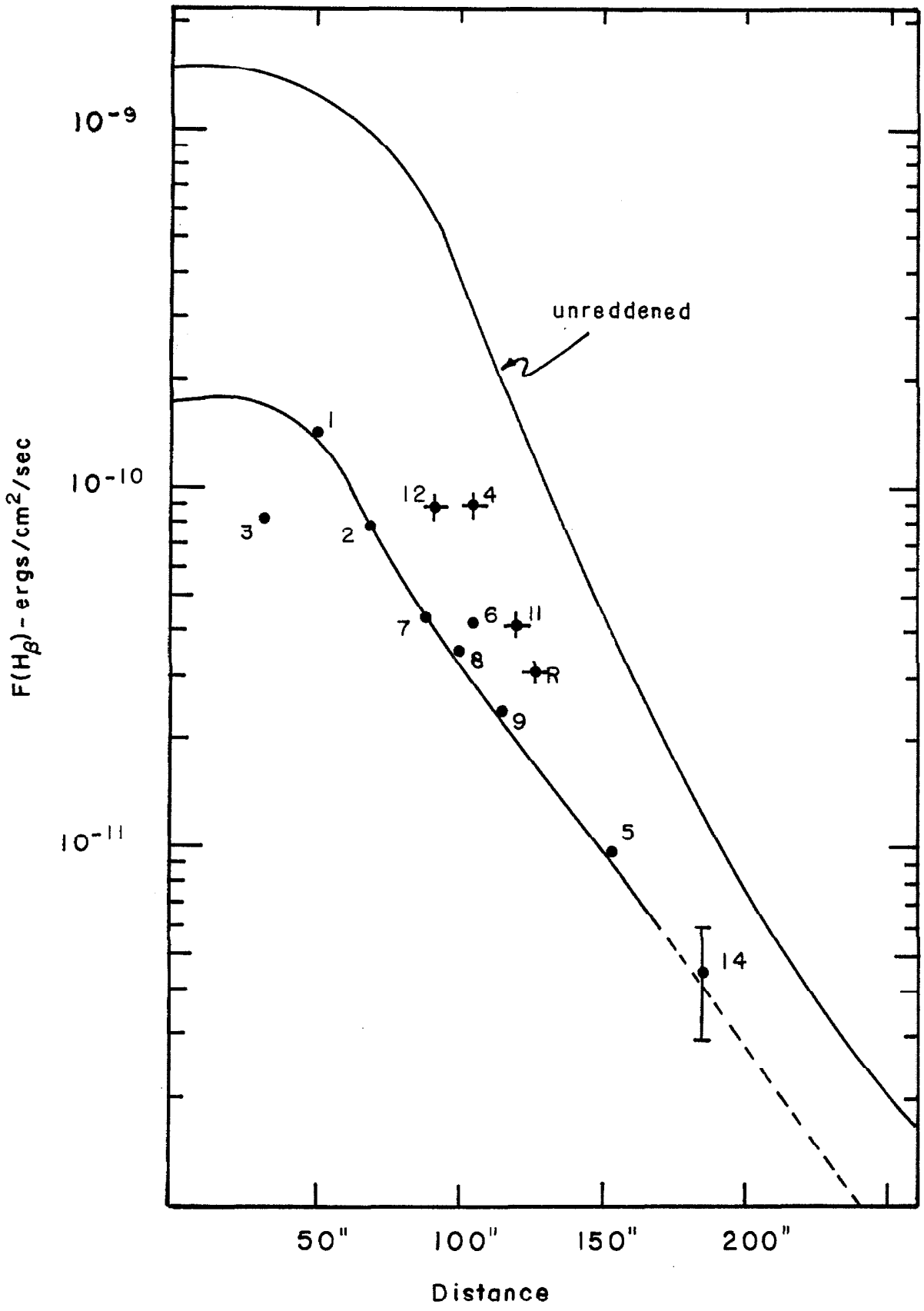
10^{-9}
10^{-10}
10^{-11}
$F(H_\beta)$ - ergs/cm^2/sec
unreddened
1
2
3
4
5
6
7
8
9
11
12
14
R
50"
100"
150"
200"
Distance

flux, at λ4861, can then be derived as a function of the distance from the center of the nebula. Table 11 gives the relevant data; the shape of the distribution is shown in Figure 5. The crosses indicate the condensations, which obviously depart from the normal distribution. The most distant point observed (number 14, not included in Table 1) lies 185 seconds of arc away from the center. This point was observed only twice, 5007, Hβ, and HΥ were the only three lines observed; due to the high noise level present at the amplification gain used, the accuracy in the absolute values is the worst of all. However, this point indicates roughly how the distribution in flux should look beyond 3'. The dotted line indicates that those values are roughly extrapolated.

The angular resolution of the radio observations of the nebula, available at the present time, are rather poor; consequently, a direct comparison with the radio distribution is difficult to make. Notwithstanding this limitation, something can be stated through the data available. If reddening is included, the central points, where the extinction is heavier, will go farther up in Figure 5 than points 5 and 14 where the reddening is smaller. Therefore, the distribution shape would resemble an exponential curve rather than a Gaussian, which is the radio distribution indicated by the work of Menon(46).

If spherical symmetry is assumed, one can integrate the optical data up to any given radius. Assuming a radius

of 20' for the nebula, the total flux at Hβ is then:

$$F_{H_\beta} \approx 2.8 \times 10^{-8} \text{ erg/cm}^2\text{.sec}$$

the flux, at 3.15 cm, as given by Osterbrock(5) is:

$$F_{3.15} = 4.8 \times 10^{-21} \text{ erg/cm}^2\text{.sec.cps.}$$

From this value and Equation 34, the flux at Hβ predicted is 1.4×10^{-7}, which is a factor of 5 greater than that derived through the integration of the reddened energy distribution at λ4861. That reduction factor of 5, corresponding to 1.7 magnitudes, is unquestionably due to the extinction produced by absorbing particles, of both nebular and interstellar character. The mean color excess of the Trapezium stars, as determined by Sharpless(47) is 0.36. With the ratio of total to selective absorption at λ_V,

$$\frac{A_v}{E_y} = 6.0$$

also derived by Sharpless(48), the absorption for light at Hβ is, accordingly

$$A_{H_\beta} = \frac{\lambda_v}{\lambda_{H_\beta}} 2.16$$

on the B-V system, $\lambda_v^{-1} = 1.83$, then

$$A_{H_\beta} = 2.47$$

This value implies a reduction factor of about 10, whereas a factor of 4.5 was derived for the nebula as a whole. The difference can be explained in terms of a central concentration of dust. This explanation is supported by the fact that the

stars, not within the Huygenean region, show a smaller color excess of about 0.23 (47) (θ^2Ori has an excess of 0.25). With this information, one can conclude that the central region, with radius of about 3', contains 2.5 times more dust than the area of the nebula outside the Huygenean region.

With this distribution of absorption, the unreddened flux at Hβ can be obtained. Figure 5 gives the distribution up to a radius of 20'. It must be borne in mind that the distribution for $Y > 4'$ is merely a crude extrapolation. If one integrates, again assuming spherical symmetry, using the unreddened curve, then

$$F_{H\beta}(r \approx 20') = 2 \times 10^{-7}$$

This flux is now larger than the one predicted. The difference might be due to the symmetry proposed. For the central region there are obvious departures from a spherical distribution in surface brightness; since, about 85 percent of that flux arises in a region within a radius of 4', the discrepancy is not due to errors in the extrapolation. Notwithstanding, the disagreement of 43 percent, the distributions shown in Figure 5 were adopted for all the computations in the present work. The emission measure, as derived from the unreddened data, is given in Figure 6.

The total absorption at λ1216, the wavelength of Ly-α, can also be estimated using the arguments presented in an earlier section. After the comparison of the optical

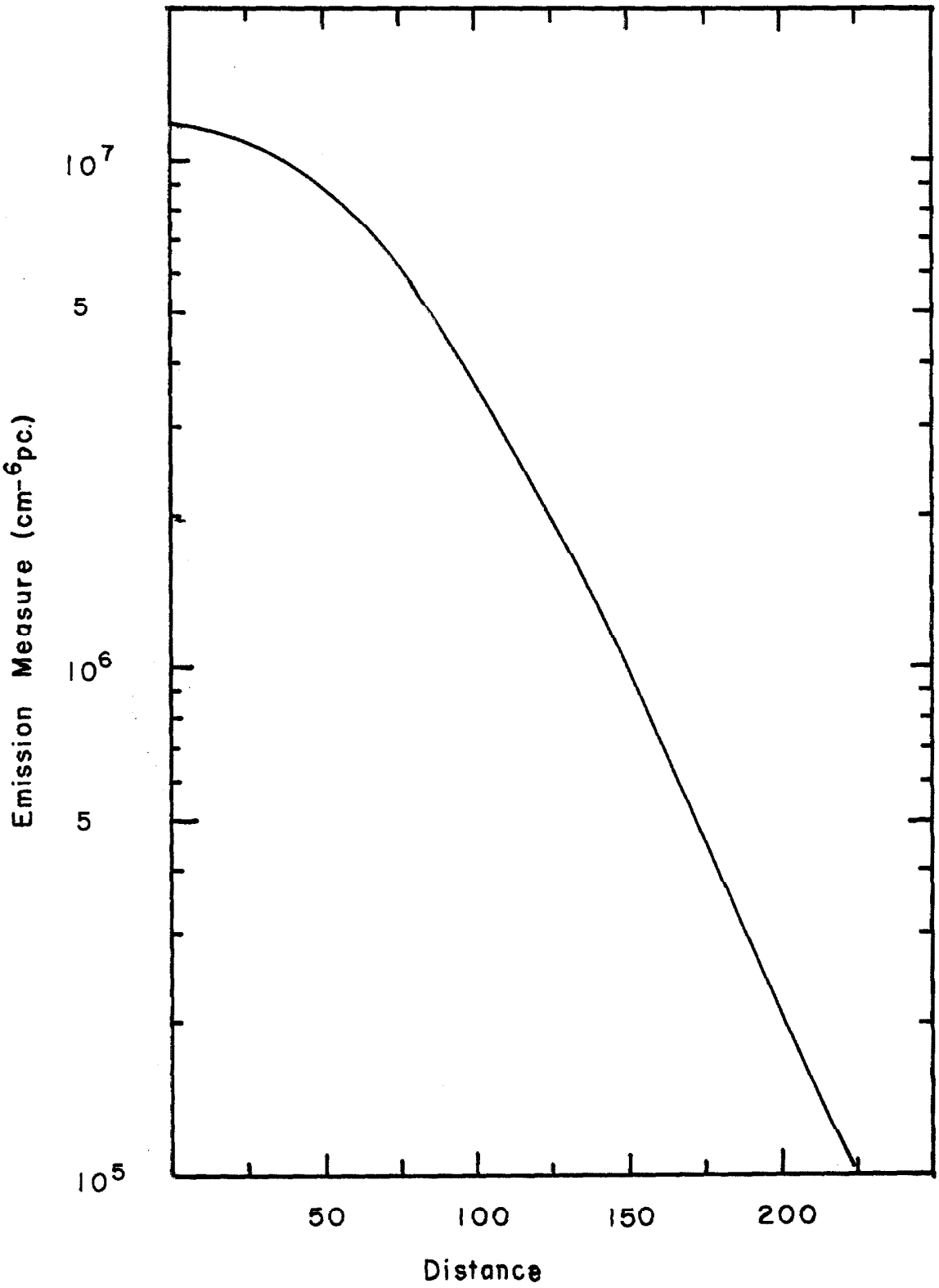
Emission Measure (cm^{-6}pc.)
10^7
5
10^6
5
10^5
50
100
150
200
Distance

Figure 6

depth, at λ3889, obtained by direct observation with that computed with Equation 21, it was concluded that the number of Ly-α scatterings, $\mathcal{Q}$ must be reduced by a factor of 330. This is equivalent of saying that, along a path length L, the Lyman-Alpha radiation is absorbed by dust, decreasing the intensity at that wavelength by the same factor. As a first approximation, we find that

$$\exp\left[\int_0^L N_S(\text{dust})\, k\,(\lambda 1216)\, ds\right] = 330 \qquad (36)$$

where N_S is the mass density of the absorbing material, and k(Ly α) is the mass absorption coefficient, which may be expresses in terms of the geometrical cross section πa^2 and an efficiency factor $Q(a,\lambda)$ in the form

$$k(\lambda) = \frac{Q(a,\lambda)\,\pi a^2}{4/3\,\pi a^3 s} = \frac{3}{4}\,\frac{Q(a,\lambda)}{as} \qquad (37)$$

where s is the density of the solid grain. Very little is known about the nature of the dust imbedded in HII regions, consequently, the knowledge of the particle size distribution is entirely unknown. Therefore, the same radius a will be assumed to be constant throughout the whole nebula. With this simplification, Equation 36 becomes:

$$0.75\, N(\text{dust})\,\frac{Q(a,\lambda)}{as}\, L = 5.8 \qquad (38)$$

If the same idea is applied to the reduction factor of 10, produced by dust at Hβ, as derived above, one obtains a relation similar to 38. The right hand side being 2.25,

therefore, we find that:

$$R(a) = \frac{Q(a, 1216)}{Q(a, 4861)} = 2.6 \quad . \qquad (39)$$

The value of $Q(a,\lambda)$ depends on the nature of the solid particles, namely size, shape, refractive index and optical and magnetic properties. Extensive computations of the efficiency factor have been carried out for various kinds of particles. Each case gives a definitive and unique variation of Q as a function of both the size of the particle and the wavelength of the incident light. Condition 39 provides an indication of the proper kind of particle.

From the higher abundance of the elements with low Z, one could expect the dust to contain dominantly H, He, O, C, N, Mg or Si. Metallic elements like Fe, Ni, and Cr would consitute a minor impurity only. Therefore, the dust must behave as a dielectric material, although a small metaliticity would be expected due to the impurities. The hydrogen and helium would evaporate off the grains, in HII region conditions, since their vapor pressures for the solid phase are extremely small. The hydrogen could remain combined with other elements through covalent bonds. In a solid, the only possibilities are: H_2O, NH_3, and CH_4, which again must have predominantly dielectric properties. Also, one can expect compounds like SiO_2, M_gO, CO, and CO_2.

Van de Hulst(22), in his review article, provides a good collection of extinction curves for various kinds of

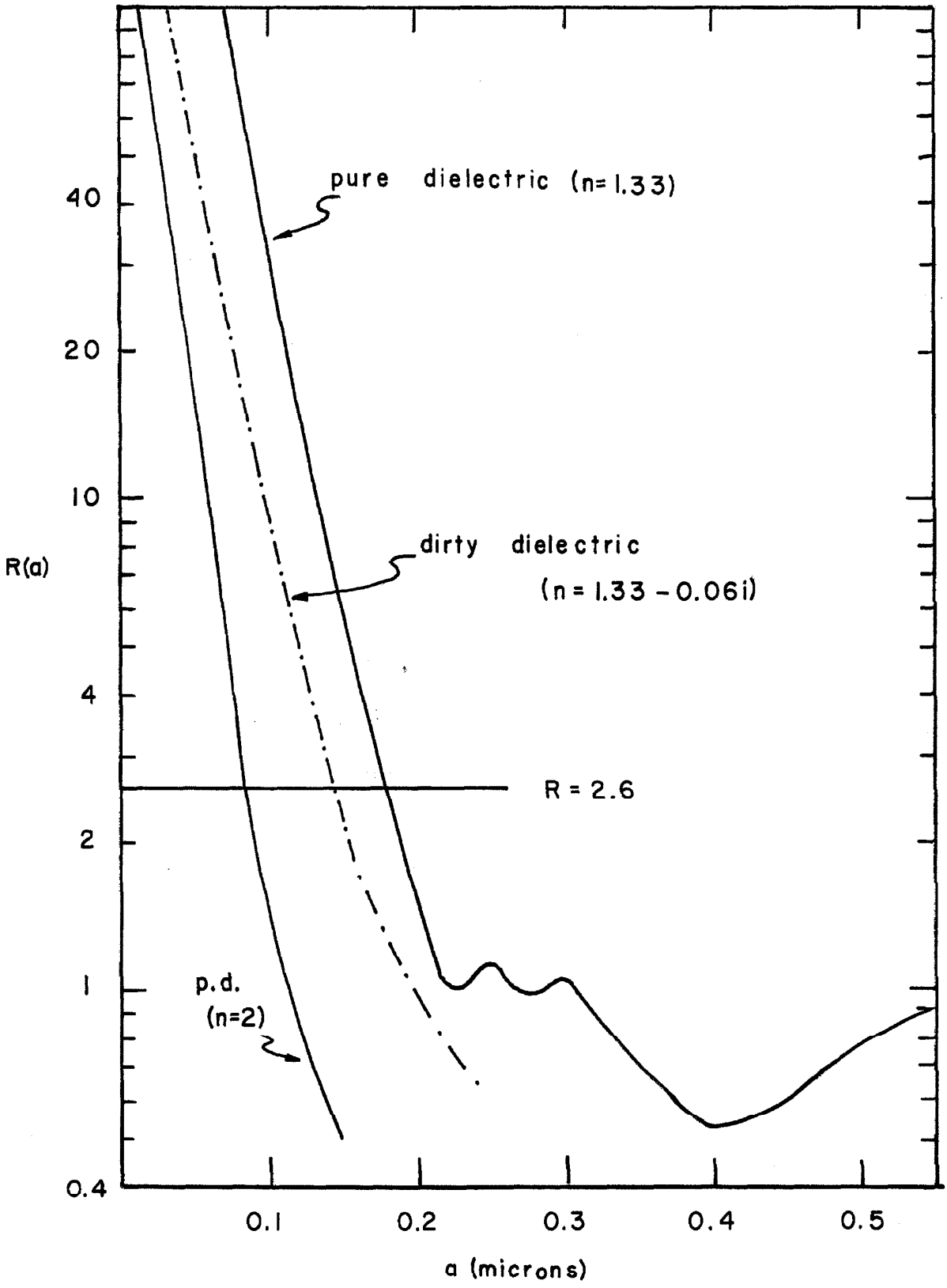
pure dielectric (n=1.33)
dirty dielectric
(n = 1.33 - 0.06i)
R = 2.6
p.d.
(n=2)
R(a)
40
20
10
4
2
1
0.4
0.1
0.2
0.3
0.4
0.5
a (microns)

Figure 7

particles. Those curves are primarily computed for spherical grains. In an HII regions, as the Orion nebula, the collisions, more frequent than in the interstellar medium, would certainly favor the sphericity of the dust particles. Figure 7 shows the variation of R as a function of particle radius, assuming spherical shape, for 3 types of grains.

a) Pure dielectrics, with a refractive index of 4/3, value for the waterdrops and close to the refractive indices of frozen ammonia (1.32, frozen CH_4 (1,26) and frozen H_2 (1.10).

b) Pure dielectrics, with a refractive index of 2.0. this high value would represent denser material, as perhaps silicates. Intermediate values of m can be easily computed by interpolating between the two curves.

c) Dirty dielectrics, that is a dielectric with metallic impurities. In this case the complex refractive index

$$m = 1.33 - 0.06i \qquad (40)$$

has been considered approximate. For this particle true absorption occurs, since electromagnetic waves are converted into heat.

Figure 7 shows that, if condition 39 holds in the nebula, the particles must have a radius in the vicinity of 0.16 microns. Moreover, particles of that size, in addition to satisfying Equation 39, assure the $1/\lambda$ dependence of the

reddening curve. It must be pointed out that the absorption of light at λ1216, as derived above, involves only the dust imbedded in the nebula, whereas the absorption at λ4861 includes both the dust in the nebula and the interstellar particles placed between the earth and Orion. This effect tends to reduce the value of R, with respect to the true value. However, an increase of R in a 20 percent would not effect at all the value of a, obtained with Figure 7.

It can be seen that particles with radius larger then 0,2 are out of the question, for otherwise the reddening curve would show a rather peculiar behavior. It could be objected, however, that the refractive index has been considered constant in a wide range of wavelengths, an assumption that cannot be supported. A direct inspection of the extinction efficiencies curves shows that Q(a,1216) always decreases with increasing indices of refraction, provided that a is larger than 0,1 micron. Since the index of refraction at λ1216 is higher than at λ4861 (if no absorption bands are present), the efficiency factor Q would tend to be lower. Those arguments hold only in the case of classical particles, however, at wavelengths in the ultraviolet regions, quantum mechanical effects begin to become important. Electron transitions, molecular dissociation, etc. are effects which again increase the efficiency factor, probably cancelling out the effects of the higher refractive index. No estimates of the latter effects can be made without introducing especulative

facts; therefore, it has been assumed that the constancy of the refractive index is a fair approximation.

On the other hand, the reddening curve seems to behave according to the $1/\lambda$ law, from λ = 3700 to λ10 000, nearly with the same slope; a fact that is supported with the close agreement between the H and He line intensities measured and the pure recombination values. The change of slope at about $1/\lambda$ = 1,8, present in the reddening curve as derived with the six-color observations, cannot be reconciled with particles with radius of about 0,16. As van de Hulst(22) pointed out, that change in slope, or the relatively small absorbing power in the ultraviolet, could be explained with particles of larger size than the ordinary ones in the interstellar medium. The smaller grains can be better explained in terms of electron collisions. That is, if the destruction of dust particles takes place through collisions with the electrons, the larger grains would be destroyed more easily. Consequently, the maximum of the particle size distribution would be shifted toward smaller sizes, increasing the absorption in the ultraviolet and blue regions of the optical spectrum, as indicated by the Paschen/Balmer line ratios (see Figure 2).

If the radius of 0,16 is considered as the representative value for the dust particles, the mass density of the solid material in the nebula can be easily derived with the use of Equation 38, which is transformed into,

$$N_s(dust) = 1.23 \times 10^{-4} \frac{s}{Q(1216)L} \qquad (41)$$

taking Q = 2.5 as the efficiency factor, which corresponds to a dielectric with a small amount of impurities, the density s is about 1.3 gr/cm^3 for a frozen gas, then

$$N_s = 6.4 \times 10^{-23} \text{ gr/cm}^3$$

The density of the gas can be derived from the surface brightness data of Table 1 and with the equation

$$10\, S_{4\beta} = \frac{L}{4\pi} \alpha_{4,2} h\nu_{4861} N_e^2 \quad . \qquad (42)$$

Taking the observations for point 1 as representative of the central region (the factors of 330 and 10 were derived for this case), one obtains

$$N_e = 5.5 \times 10^3 \text{ electrons/cm}^3 \quad .$$

Using the hydrogen to helium ratio found in an earlier section, one can obtain the mass per free electron, and the mean value of the ratio between the densities of gas and dust is, for the central region of the Orion nebula;

$$\frac{N(gas)}{N(dust)} \approx 200 \qquad (43)$$

It should be borne in mind however, that this ratio might show appreciable variations for different points throughout the nebula.

This value is two times greater than the mean ratio found in the Taurus-Orion Dark Nebulae Complex by the 21 cm. survey (49). Furthermore, this ratio indicates the possibility of a steady progression going from low values for the ratio between the densities of gas and dust grains for the interstellar medium (close to the galactic plane), to the average value for diffuse nebulae (Orion), to a still lower ratio for the dense and dark nebular complexes.

D) Density Fluctuations

A direct inspection of Figure 1 would clearly indicate that the Orion nebula cannot be considered as a homogeneous distribution. The effects of those density fluctuations are of the utmost importance in the interpretation of the observations, both in the optical range and in the radio region. Moreover, the stratification in the line formation mechanisms proposed in Section 2 of this chapter needs, for its support, a direct knowledge about the character of the density fluctuations in the nebula.

Osterbrock(5), utilizing the intensity ratio of the lines λ3726 and λ3729 of (OII), determined the electron density distribution of the nebula as function of the distance from the center. A maximum value of $1.8 \times 10^4 cm^{-3}$ was found for the center; his observations extended up to distances of 24 minutes of arc from the Trapezium. In those outer regions he observed elements with densities of the order of 250 cm^{-3}. Assuming homogeneity in the nebula, he then computed the

radio flux at six different wavelengths, from 3.15 cm where the nebula behaves as an optically thin layer, to 350 cm, where the radio emission is not any longer proportional to the radiation in the hydrogen lines. The computed fluxes were several times the observed. Therefore, the idea of inhomogenities was introduced as a mathematical tool; assuming a model with condensations distributed at random, through a spherical region, the fluxes were recomputed using now an effective radius αL rather than only L. In this way, α is defined as the fraction of the length of the average line of sight occupied by condensations. The introduction of α makes the optical depth decrease relatively to the homogeneous model. With a value of α of 1/30.3, the agreement with the observations was better, although not complete. The origin of the remaining discrepancy will be explained later in this section.

Münch and Wilson(6) rejected the spatial arrangement of gas and stars proposed by Würm(7) for the Orion nebula, already discussed in Section 2, on the basis of the existence of density fluctuations. Their analysis is interesting because in the depopulation mechanisms of the 2^3S level involved in their work, the ionization by Ly-α radiation was not considered. With similar agreements to those given in Section 2, they derived:

$$N_e^2 D = 1.7 \times 10^4 \left(1 + 4.4 \times 10^{-4} N_e + 0.077 r^{-2}\right) \text{cm}^{-6}\,\text{pc} \qquad (44)$$

using the observed strength of λ3889 in absorption. It can be seen that with $N_e = 1.8 \times 10^{+4}$, $\gamma^2 = 0.1$, the emission measure is about 100 smaller than the surface brightness derived for the center of the nebula (see Figure 6). They explained the discrepancy by considering elements capable of producing the HeI λ3889 absorption, with such a short effective path length, that the surface brightness is 100 times smaller than in the large scale. With the distance γ to the ionization source being 0.32 pc, for the central regions where electron density is close to $10^4 cm^{-3}$, $D \approx 6 \times 10^{-3}$ pc. For the outer regions, with $N_e \approx 750 cm^{-3}$, $D \approx 0.1$, but the distance γ needs to be close to 1 pc. With these quantities, $\alpha \approx 1/60$, for the dense elements; whereas $\alpha \approx 1/10$ for the outer regions. Due to the size of the elements producing the lines, it was further concluded that no correlation could be expected between the radial velocities of the emission lines and those of the λ3889 absorption lines.

However, as is shown in Table IX, there is a correlation between the velocities. Furthermore, when the depopulation rate n_α, due to photoionization by Ly-α quanta, is included in Equation 44, one obtains, taking into account the extinction of Ly α by dust:

$$N_e^2 D = 5.4 \times 10^6 (2.08 + 0.002 \times 10^{-6} N_e + 1.7 \times 10^{-4} \gamma^{-2}) \qquad (45)$$

using $N_e = 2.10^4$, the emission measure indicated by the λ3889 line in absorption (W = λ 0.2), at the center of the nebula is:

$$D N_e^2 = 1.25 \times 10^7 \quad cm^{-6} pc.$$

value that is in excellent agreement with the emission measure derived with the Balmer emission lines. In this case $\alpha < 1/2$ (see Figure 6).

The latter value of α is quite different from that originally assumed by Osterbrock ($\alpha = 1/30.3$) Moreover, the emission measure at the center of the nebula, as derived from the density distribution given by the $\lambda(3727)$ lines, averaged over a circle of radius 0.65, turns out to be 5.6×10^7. Comparing with the corresponding value for point 1, $\alpha \approx 1/5$. Evidently, a closer approach to the problem of density fluctuations must be carried out.

Let the nebula be considered as a spherical cloud with radius R, and assume that the electron density can be expressed as a function of ℓ, the distance from the center.

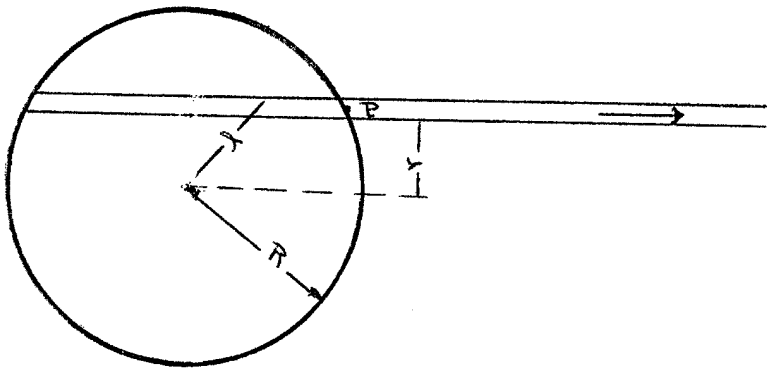

Figure 8

Then the reddened emission measure E at a point P, located at Y minutes of arc from the center, according to Figure 7, is

$$E(Y) = \int_0^{\sqrt{R^2-Y^2}} N_e^2(\ell)\, e^{-\tau(s)}\, ds = \int_0^{\sqrt{R^2-Y^2}} N_e^2[(R^2-Y^2)^{1/2}]\, e^{-\tau(s)}\, ds \qquad (46)$$

E(Y) has been determined by direct observation, therefore, the solution of the integral Equation 46, which is a Volterra equation of the first kind, can be solved by numerical methods, leading to the knowledge of the function $Ne^2(\ell)$. The solution would require $\tau(s)$ to be given, which in turn implies that the density distribution of the solid matter, N(s) is known. Although it is clear that the dust is heavily concentrated toward the center of the nebula, its distribution as a function of distance cannot be determined. Consequently, one approximation, to simplify the problem, must be introduced; namely, that $\tau(s)$ is a constant. The exponential can be transferred to the left size of Equation 46, and the unreddened emission measure $\xi(Y)$, as given in Figure 6 can be used.

$$\xi(Y) = \int_0^{\sqrt{R^2-Y^2}} N_e^2\,(\sqrt{R^2-Y^2})\, ds$$

The integration carried over half the sphere only, since that is what is observed. For otherwise, the far side of the nebula could be observed. When theoretical radio

fluxes are to be computed, the whole sphere must be considered. Using ℓ as a variable, one has

$$\mathcal{E}(r) = \int_R^r \frac{N_e^2(\ell)\, \ell\, d\ell}{\sqrt{\ell^2 - r^2}} \quad . \qquad (47)$$

The form of this equation is similar to the classical Abell equation, which is:

$$f(x) = \int_a^x \frac{v(z)}{(x-z)^p}\, dz \qquad (48)$$

where

$$0 < p < 1 \quad \text{and} \quad a \leq x \leq b$$

the solution is (see Whittaker, Modern Analysis, page 229)

$$v(z) = \frac{\sin p\pi}{\pi} \frac{d}{dz} \int_a^z \frac{f(x)\, dx}{(z-x)^{1-p}} \qquad (49)$$

with the change of variable

$$R^2 - r^2 = \omega \quad ; \quad R^2 - \ell^2 = v$$

the integral Equation 47 becomes

$$\mathcal{E}(\omega) = -\int_0^\omega \frac{\frac{1}{2} N_e^2(v)\, dv}{(\omega - v)^{1/2}}$$

which is of the desired form. Consequently, one has

$$N_e^2(v) = \frac{d}{dv} \frac{1}{\pi} \int_0^v \frac{2\, \mathcal{E}(\omega)}{(v-\omega)^{1/2}}\, d\omega$$

carrying out the integration by parts first, and then taking the derivative

$$N_e^2(\upsilon) = -\frac{2}{\pi}\int_0^{\upsilon} \frac{d\xi(\omega)}{d\omega}\,\frac{d\omega}{(\upsilon-\omega)^{1/2}}$$

And finally:

$$N_e^2(\lambda) = \frac{2}{\pi}\int_{\lambda}^{R} \left|\frac{d\xi(r)}{dr}\right| \frac{dr}{(r^2-\lambda^2)^{1/2}} \qquad (50)$$

Following the same arguments given by Osterbrock, the density square given by 50 must be equal to the projected $Ne^2(\gamma)$, obtained through the (OII) doublet, multiplied by the condensation parameter α. The values of $\frac{d\xi(r)}{dr}$, can be determined directly from Figure 6. The integration was carried out using the scale 1' = 0,131 parsec. As has been said before, the values for $\gamma > 4'$ were obtained by a rough extrapolation, and the integration for $\ell > 6'$ is meaningless simply because in those cases the errors in the gradient of $\xi(\gamma)$ become very serious.

The parameter α, as defined by Osterbrock, is then merely the ratio:

$$\alpha(\lambda) = \frac{\frac{1}{\pi}\int_{\lambda}^{R} \left|\frac{d\xi(r)}{dr}\right| \frac{dr}{(r^2-\lambda^2)^{1/2}}}{\left[N_e^2(\lambda)\right]_{proy.}} \qquad (51)$$

Table 12 gives the results of the computation,

TABLE XII

ℓ	$N_e^2 \times 10^{-6}$ Eq.50	$N_e^2 \times 10^{-6}$ [OII]	α^{-1}
1'	36,2	108	5,9
2'	5,2	34	13,1
3'	0,80	9,2	23
4'	0,16	3,6	45
5'	0,11	2,25	60
6'	0,042	1,58	79

and indicates, beyond any doubt, that the parameter α decreases outward. This kind of variation is produced by a nebula with density fluctuations, which vary in size as a function of the distance from the center. That is, the nebula is more homogeneous in the center than in the outer regions. It is clear that the density distribution depends largely on the initial conditions (before the O6 star was born). However, this increasing inhomogeneity in the outer layers could be explained in terms of the interaction of the expanding gas with the highly disordered medium around the nebula. This interaction would certainly corrugate the ionization front leading to fragmentation. The closer to the ionozation front, the larger the inhomogeniety in the electron density.

Osterbrock's observations cover a large region of the nebula, in principle his projected electron density dis-

tribution is more accurate than the distribution obtained here, where only 5 points were used to derive the surface brightness distribution. However, the character of the variation of α is not far from the truth and can be used to repeat Osterbrock's computations. Assuming $\alpha^{-1} \approx 200$ for R = 24', and using the data of Table XI, integrations were carried out with the IBM 7090 computer of the California Institute of Technology. The fluxes at six radio frequencies were computed using the same equations of Osterbrock's paper (5). The results are in good agreement with the observed values, although still a little higher at large wavelengths. Table XIII gives the comparison. The differences are smaller than the errors involved in the radio observations; then it can be concluded that the discrepancy between theory and observations, found by Osterbrock, can be satisfactorily explained in terms of the decrease of α with distance from the center.

TABLE XIII

		COMPUTED ergs/cm^2 sec cps x 10^{21}		
λ(cm)	Observed Flux	α=1	α=1/30.3	$\alpha(\gamma)$
3.15	4.8	190	5.4	4.5
9.4	5.8	180	5.8	5.2
21.0	4.6	150	6.1	4.0
50	3.0	94	6.0	3.2
75	2.3	62	5.4	2.65
350	0.9	43	2.0	1.0

This kind of distribution is for elements in the large scale; that is, elements with much larger dimensions than those where the HeIλ3889 in absorption is produced. If the Ly-α quanta did not play a significant role in the depopulation of the 2^3S level, one would conclude that the small elements behave in the opposite direction of the large elements. Its α' would then be small in the central regions, and large in the outer parts of the nebula, which is physically impossible.

E) The Nebular Continuum Spectra

In addition to the observation of the emission lines, some photoelectric measurements of the continuous spectra were carried out. The accuracy of these observations is not as good as that obtained with the emission lines, because the dark current was not measured very frequently, and occasional drifts could introduce appreciable errors. For point 1, the brightest of all, the measures were performed more systematically and consequently the errors are smaller than for the other points. For this reason, only the observations of point 1 will be discussed.

There are five possible sources of continuous emission; namely,

1) Recombination of ionized atoms. Only H and He would be important.
2) Free-free emission.
3) Two-photon emission. Only H is important.

4) Electron scattering,

5) Scattering and reflection of stellar light by dust particles.

Processes 1 and 2 can be computed directly and no further comments are needed. Although for process number 3, the rate of emission is given by recombination calculations, some doubts have arisen in the past about whether or not the Ly-α photons, by electron collisions, would be degraded to two continuum photons of lower energy. This question can be ruled out with the following discussion. The number of Ly-α photons per unit volume is (see Equation 9) $(1-X)\alpha_\beta N_e^2$, since an average Ly-α quanta is scattered Q times before it leaves the nebula, the rate of the 2p to 2s collisional deexcitation is

$$H = (1-X)\,\alpha_B\, N_e^2\, \frac{\langle \sigma v \rangle_{2p-2s}}{A_{21}}\, N_e\, Q \times 0.92 \qquad (52)$$

since

$$N_H = 0.92\, N_e$$

Therefore, the energy emitted due to the two-photon emission process, including the electrons recombining into the 2s level is

$$E_{2q} = 0.92\, N_e^2 \left[0.66\, A_{2q}\, \alpha_B\, \frac{\langle \sigma v \rangle N_e}{A_{21}}\, Q + \gamma(2q)\right] d(h\nu) \qquad (53)$$

where A2q is the probability of the $2s \rightarrow \ell s$ optical transition, and $\gamma_o(2q)$ is the continuum recombination coefficient for the same process. With $Q = 8 \times 10^5$, and $N_e = 10^4$ cm^{-3}, the first

term in the bracket is, for Te = 10^4 K, equal to 3.14 x 10^{-15} sec^{-1}. This value must still be decreased by at least a factor of 100 due to the dust extinction; since the $\gamma_0(2q)$ coefficient is always of the order of 10^{-14}, one can safely conclude that the Ly-α radiation in the nebula cannot originate a significant production of two-photon emission. This will not be the case for planetary nebulae where N_e is higher and Q is not decreased by dust particles.

Therefore, the 3 first processes can be represented by the expression

$$E_c = \frac{92\, N_e^2 \left[\gamma(H^+) + 0.1\gamma(He^+) + \gamma_0(2q)\right] d(h\nu)}{0.92\, N_e^2\, \alpha_{4,2}\, h\nu(H_\beta)} \qquad (54)$$

which is in units of $H_\beta \left(I(H_\beta) = 100\right)$. In the above equation $\gamma(H^+)$ represents the continuous recombination coefficient for free-free transitions plus recombination, $\gamma(He^+)$ for recombination of the HeII atoms; after some manipulation:

$$E_c = 1.62 \times 10^4\, \lambda^{-2} \left[0.1\gamma(He^+) + \gamma(H^+) + \gamma(2q)\right] \Delta\lambda \qquad (55)$$

where λ and $\Delta\lambda$ are in microns. The values for the γ's have been tabulated by Seaton(50) for various temperatures. The bandwidth $\Delta\lambda$, used in the observations was 10 A. Calculations have been carried out for various values of λ and the results are compared with the observed values in Table XIV.

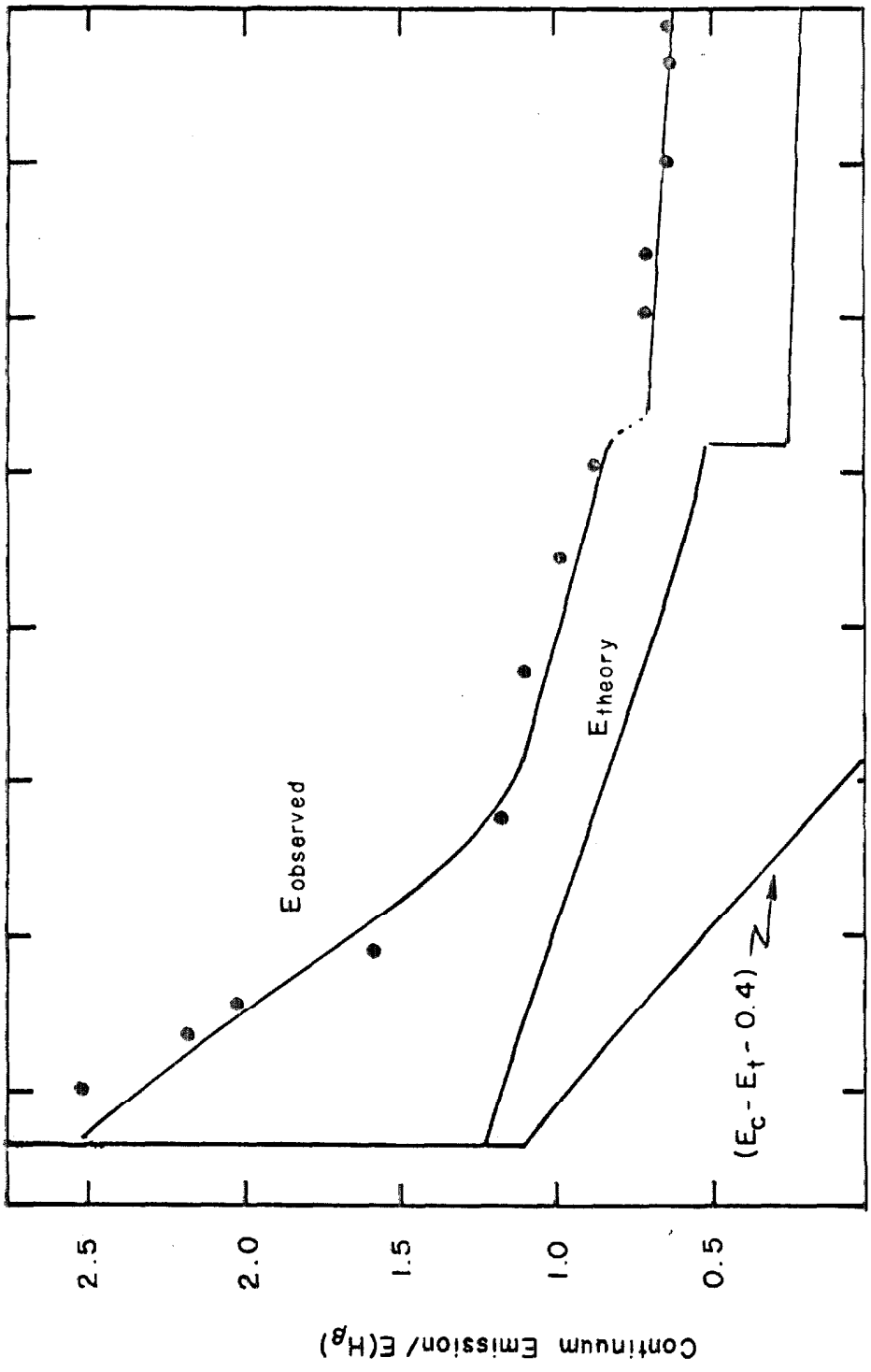
Continuum Emission/ E(Hβ)
2.5
2.0
1.5
1.0
0.5
0.4
0.5
0.6
0.7
0.8
0.9
1.0
λ (microns)
Eobserved
Etheory
(Ec - Et - 0.4)

Figure 9

TABLE XIV

λ	E_c	Tc=8200 $E_{Obs.}$	Tc=9600 $E_{Obs}-E_c$	Tc=12200 K $E_{Obs}-4-E_c$
3650^+	1,33	2,55	1,20	0,80
5000	1,00	1,7	0,70	0,30
5800	0,85	1,3	0,45	0,05
8192^+	0,55	0,85	0,30	0,10
8192	0,28	0,75	0,50	0,10
9115	0,25	0,65	0,40	0,05
10000	0,24	0,65	0,41	0,05

It can be seen from Table XIV, and also from Figure 9, that there is the possibility of a small component of electron scattering. As is well known, this mechanism is independent of wavelength and can possibly be reconciled with the almost constant flux beyond λ8200.

The color temperature has been determined for the three components and is given at the top of Table XIV. Those temperatures are measured in the visual region, at λ5400. In the blue the temperatures are higher. Similar measures were carried out by Greenstein(2), and by Barbier(51) in the blue region of the nebular spectrum. The temperature in the same region, as determined from Figure 9, is about 12 300 K, in good agreement with the 11 5000 K determined earlier by Greenstein, but about 2 times the value found by Barbier.

In the same units, the value of the flux at λ3600 is close to 11,1 if the corresponding value at $\lambda 3650^+$ is

2.6 as extrapolated in Figure 9, the Balmer discontinuity D, defined as:

$$D = \log_{10} \frac{E(3650^-)}{E(3650^+)} \qquad (56)$$

is 0.62. Since D is a function of the electron temperature, the value of the latter quantity can be obtained. Using the data provided by Seaton(50), one finds that Te = 12000 K. It will be shown in the next chapter, that the electron temperature at the central regions is close to 9000 K. The disagreement can be explained if one accepts the existence of the component of electron scattering emission. Subtracting 0.40 indicated by Table XIV, the Balmer jump is now 0.71, which indicates that the temperature is 9 5000 K.

The constancy of the flux, beyond λ8200, could also be produced by a systematic error independent of wavelength, such as a calibration error at Hβ, and since it is only 0.4 percent of I(Hβ), it could not be detected through the emission line intensity ratios. However, the other points seem to behave differently. The flux at λ > 8200 for those points is always smaller than 0.40, in units of Hβ.

F) The Mass and the Age of the Orion Nebula

The emission measure can provide the root mean square electron density by the expression

$$N_e(\text{rms}) = \left(\frac{\text{EM}_{\text{center}}}{L} \right)^{1/2} \qquad (57)$$

The mass density is:

$$\rho = (N_H + 4N_{He})\, M_H = 1.26\, N_e M_H \quad . \qquad (58)$$

Then, the mass of the nebula assuming spherical symmetry, is given by

$$M = \frac{4}{3}\pi L^3 \rho \approx 27\, M_\odot \quad . \qquad (59)$$

The mass of the Orion Nebula can also be obtained with the electron density distribution given by Osterbrock. It was found in Section 7, that the projected density, as determined by the [OII]-ratio, can be related to the density corresponding to a smooth nebula by:

$$N_e(r) = \left[N_e(r)\right]_{proj} (2\alpha)^{1/2} \quad . \qquad (60)$$

Therefore, the mass is now given by:

$$M = 1.26\, M_H\, q\, 4\pi \int_0^{20} \left[N_e(r)\right]_{proj.} \left[2\alpha(r)\right]^{1/2} r^2\, dr \qquad (61)$$

where q is the scale factor; at 450 pc, after the numerical integration of Osterbrock's distribution of electron density:

$$M \approx 30\, M_\odot$$

in excellent agreement with the above determination. The amount of dust is then

$$M \approx 0.15\, M_\odot$$

The age of the nebula can be estimated from the arguments given at the end of Section 2. It was shown that there was a difference of about 18m/sec, in velocity between the outer regions where the HeI λ3889 is formed and the central regions. The inverse of this gradient of velocities would give a fair estimate of the age, then

$$\tau = \frac{\Delta s}{18^{km}/_{sec}} \quad . \qquad (62)$$

Therefore, with Δs about 10^{18}cm, and if no large changes in expansion velocities have occurred in the past, during long intervals of time, the time elapsed since the stars began to ionize the gas is 1.8×10^4 years. This rough estimate is in close agreement with the age of 10^4 years derived by Kahn and Menon(52), using different arguments. Furthermore, one might count with the fact that those intervals of time are of the same order of magnitude as the Kelvin contraction times, as derived by Hayashi(53). Following the latter author, the time scale for the contraction time is:

$$\tau_c = 10^7 (M/M_\odot)^2 (L_\odot/L)(R_\odot/R) \qquad (63)$$

if for θ'C Ori one adopts (56)

$$\mathrm{Log}(M_\odot/M) = 1.5 \ , \ \mathrm{Log}(LL_\odot^{-1}) = 4.75 \text{ and } \mathrm{Log}(RR_\odot^{-1}) = 1.0$$

the Kelvin contraction time is 1.3×10^4 years.

CHAPTER IV

FORBIDDEN LINE EMISSION

a) General Theory

According to the traditional terminology in atomic spectroscopy, all the lines which violate the selection rules for electric dipole radiation, are denoted as forbidden lines. Electric dipole transitions, which can only be induced by the presence of an electric field, whether external or produced by the atomic nucleus, are also labeled as forbidden lines. In the nebular spectra, the most important forbidden lines are produced either through electric quadrupole transitions or magnetic dipole radiation. The nature of each type of radiation depends on the energy levels from whence the line arises.

As a general rule, the transition probabilities for these forbidden lines are very small compared with the electric dipole transitions. In some extreme cases (the nebular lines of OII), the transition probabilities are so small that the effect of the second kind collisions must be taken into account. To illustrate this point, let us take a two level atom. Let q_{12} be the collisional excitation rate, and q_{21} the deactivation rate, then the emission per unit volume, in the absence of a radiation field is:

$$E_{21} = N_2 A_{21} h\nu_{21} = N_1 P q_{12} h\nu_{21} \qquad (64)$$

where p is:

$$p = \frac{1}{1 + q_{21} A_{21}^{-1}} = (1 - b_2) \qquad (65)$$

b_2 is the factor which measures the departure from thermodynamic equilibrium. For a two-level atom, it is given by:

$$b_2 = \frac{q_{21}}{q_{21} + A_{21}} \quad ,$$

When the density is such that $A_{21} >> q_{21}$, the second kind collisions are not important. In this condition, the so-called low density limit, every collisional excitation is followed by the emission of a photon. For most of the lines in the nebular spectra that is the case. However, for the nebular lines of OII and the transauroral of SII, the transition probabilities are of the same order of magnitude as q_{21}, provided that the electron density is close to 10^4; consequently, p is less than unity and according to Equation 64 the collisional deactivation starts weakening the line. Eventually, when the electron density increases $q_{21} >> A_{21}$ and the emission is close to zero. That is, the population of the two levels is only determined by collisions, which is the case in thermodynamic equilibrium ($b_2 = 1$). In other words, the effect of the second kind collisions is to decrease $N_2 A_{21}$ by the factor p. Although this is not exactly true when more levels are introduced, still the second kind collisions decrease the intensity of the forbidden lines, for otherwise these lines could be observed in the laboratory.

In this chapter, the two-level atom approximation has been used for the SII and OII nebular lines.

What has been said above holds for all forbidden lines, and for the permitted ones as well. There is however, a basic difference between the two types of lines. The quadrupole and magnetic dipole transitions arise from atomic levels of energy with mean lifetimes of the order of minutes, or even longer. On the other hand, the levels, from which electric dipole transitions occur, have very much shorter lifetimes; in the case of hydrogen, for instance, the mean lifetime is of the order of 10^{-8}sec. Therefore, the second kind collisional rate would provide the basic difference, namely that the electron density needed to establish a Boltzmannian distribution among the atomic levels is quite different in each case. For the metastable states, the density is of the order of $10^{6,5}$ for the nebular lines discussed here; whereas for the hydrogen lines, the density is close to 10^{13}.

The forbidden lines to be considered here are produced from transitions between low-lying terms of certain ions, which have lower levels separated from the ground state by 3 or 4 ev. These levels are populated by electron collisions from the ground state. More specifically, the various lines arise from transitions among the terms of the ground state configurations, namely p^2, p^3, or p^4, which in turn are split in three terms: ^3P, ^1D, and ^1S for the p^2 and p^4 configuration and in ^4S, ^2D, and ^2P for the p^3.

The population of each term would depend on collisional cross-section and optical transition probabilities. If the latter quantities are provided, the population can be computed as a function of electron temperature and density in the following manner.

Let the three terms be denoted by k = 1, 2, and 3 in order of increasing excitation energy. The collisional excitation rate for a positive ion is given by the well-known relation:

$$q_{ij} = 8.63 \times 10^{-6} \frac{N_e \Omega(i,j)}{T_e^{1/2} (2J_i+1)} e^{-\frac{E_j - E_i}{kT_e}} \qquad (66)$$

similarly, the collisional deactivation rate, since Ω is symmetrical, is

$$q_{ji} = 8.63 \times 10^{-6} \frac{N_e \Omega(i,j)}{T_e^{1/2} (2J_j+1)} . \qquad (67)$$

In order to condense the notation, let Γ_{ij} be

$$\Gamma_{ij} = N_e q_{ij} + A_{ij} \qquad (68)$$

which is the total rate of downward transitions, from term j to term i. Recombination is not important for the population of the terms, from which the lines arise, for otherwise the lines arising from excited levels would be observed. Therefore these ions, with low-lying metastable levels, can be considered as consisting of only three terms. If one assumes steady conditions, the following equations,

balancing losses and gains of population for each term, are obtained:

for term 1

$$N_1 (q_{12} N_e + q_{13} N_e) = N_2 \Gamma_{21} + N_3 \Gamma_{31} \qquad (69a)$$

and similarly for the other two terms

$$N_2 (q_{23} N_e + \Gamma_{21}) = N_1 N_e q_{12} + N_3 \Gamma_{32} \qquad (69b)$$

$$N_3 (\Gamma_{31} + \Gamma_{32}) = N_1 N_e q_{13} + N_2 N_e q_{23}, \qquad (69c)$$

From these equations, the ratios N_3/N_1 and N_2/N_1 can be obtained, if one assumes a modified Boltzmann distribution as given by

$$\frac{N_i}{N_1} = b_i (N_e, T_e) \frac{\omega_i}{\omega_1} e^{-\frac{h\nu_{i1}}{kT}} \qquad (70)$$

where b_i, measuring the departure from the thermodynamic equilibrium, is a factor to be determined. Using equations 66 to 69, we obtain

$$b_2(N_e, T_e) = \frac{\Omega(1,2)\left(1+\frac{\Gamma_{31}}{\Gamma_{32}}\right) + \Omega(1,3) e^{-\frac{14388}{\lambda_{32} T_e}}}{1.17\times10^5 \frac{T_e^{1/2}}{N_e} \omega_2 \Gamma_{21} \left(1+\frac{\Gamma_{31}}{\Gamma_{32}}\right) + \frac{\Gamma_{31}}{\Gamma_{32}} \Omega(2,3) e^{-\frac{14388}{T_e \lambda_{32}}}}. \qquad (71a)$$

And for the term 3:

$$b_3 (N_e, T_e) = \frac{8.64\times10^6 N_e}{T_e^{1/2} \omega_3} \cdot \frac{\Omega(1,3) + b_2 \Omega(2,3)}{\Gamma_{31} + \Gamma_{32}} \qquad (71b)$$

when Ne is large, these two factors become unity, as is

the case of thermodynamic equilibrium, when the population distribution among the various levels is determined only by collisions. The factor b_2 has been plotted in Figure 10, for OII, SII and NII as a function of electron density, for Te = 10^4 K. The variation for $\left[NII\right]$, when Te = 10^5, is also plotted to illustrate that these factors are not very sensitive to temperature. As can be noticed, b_2(OII) becomes almost unity at densities much smaller than those required for the same factor, for the OIII atom.

All the calculations in these chapters were carried out using the expressions 71a and 71b. Tables of these factors, produced through the IBM 7090, were obtained for all the elements, which have available atomic parameters, for various values of Ne and Te.

b) The Determination of Electron Temperature

In principle, any intensity ratio of the lines arising from Term 3 to those originating from term 2 would provide a relation between the electron density and the temperature. As shown in Figure 10, the density is an important factor in determining the value of the ratio, and consequently, the electron density must be known if the electron temperature is to be determined. Although the density can be obtained by many different methods, the problem of stratification must be taken into account. That is, the same element lines should be used for both determinations - that of density and that of electron temperature. As will be discussed

Figure 10

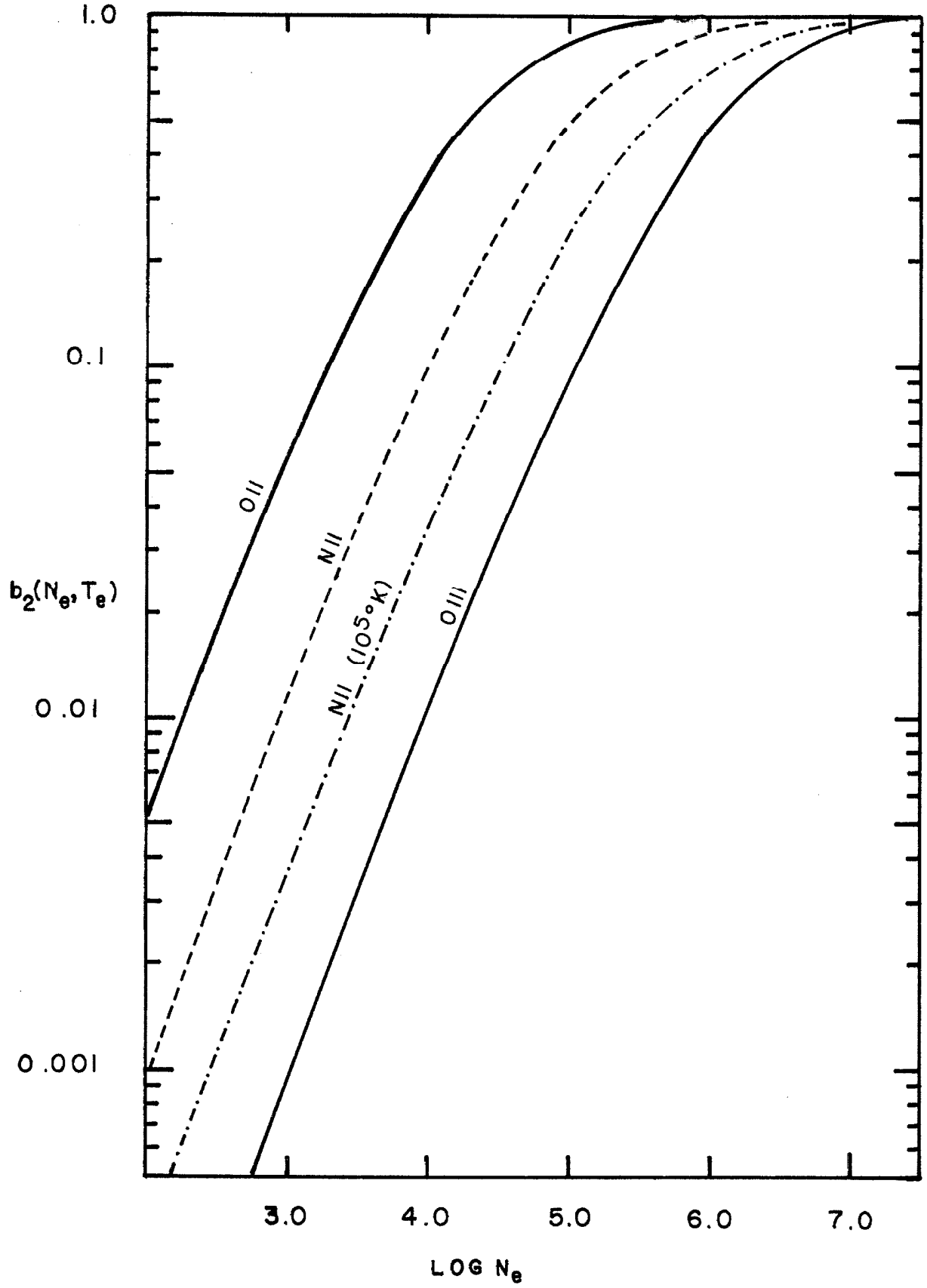

later in this chapter, the density fluctuations set the limitation, introducing an additional unknown variable - the size of the density fluctuations.

Although that is true for most of the ions producing forbidden lines, [OIII] is a fortunate exception. The b_2/b_3 ratio is practically constant for a wide range in electron densities as shown in Table XV. Consequently,

TABLE XV

	b_2/b_3		
N_e	Te=5500	Te=10^4 K	Te=2.10^4 K
10^2	119	120	121
10^3	118	120	121
5.10	116	117	120
10^4	112	113	117
$1.5x10^4$	110	112	116
$2x10^4$	109	110	113

the corresponding line ratio is, for all practical purposes, function of Te only, using Equation 69, it is given by:

$$r_{om} = \frac{I(5007+4959)}{I(4363)} = \frac{N_2\left(\frac{A_{5007}}{5007} + \frac{A_{4959}}{4959}\right)}{N_3 \frac{A_{4363}}{4363}} = \frac{b_2}{b_3} e^{+\frac{32900}{T_e}} \cdot C \quad . \quad (72)$$

Introducing the proper constants and using Table XV, C is 0.076. The electron temperature is then given by:

$$T_e = \frac{14\,330}{\log_{10} r_{om} - 0.9} \quad (73)$$

Figure 11

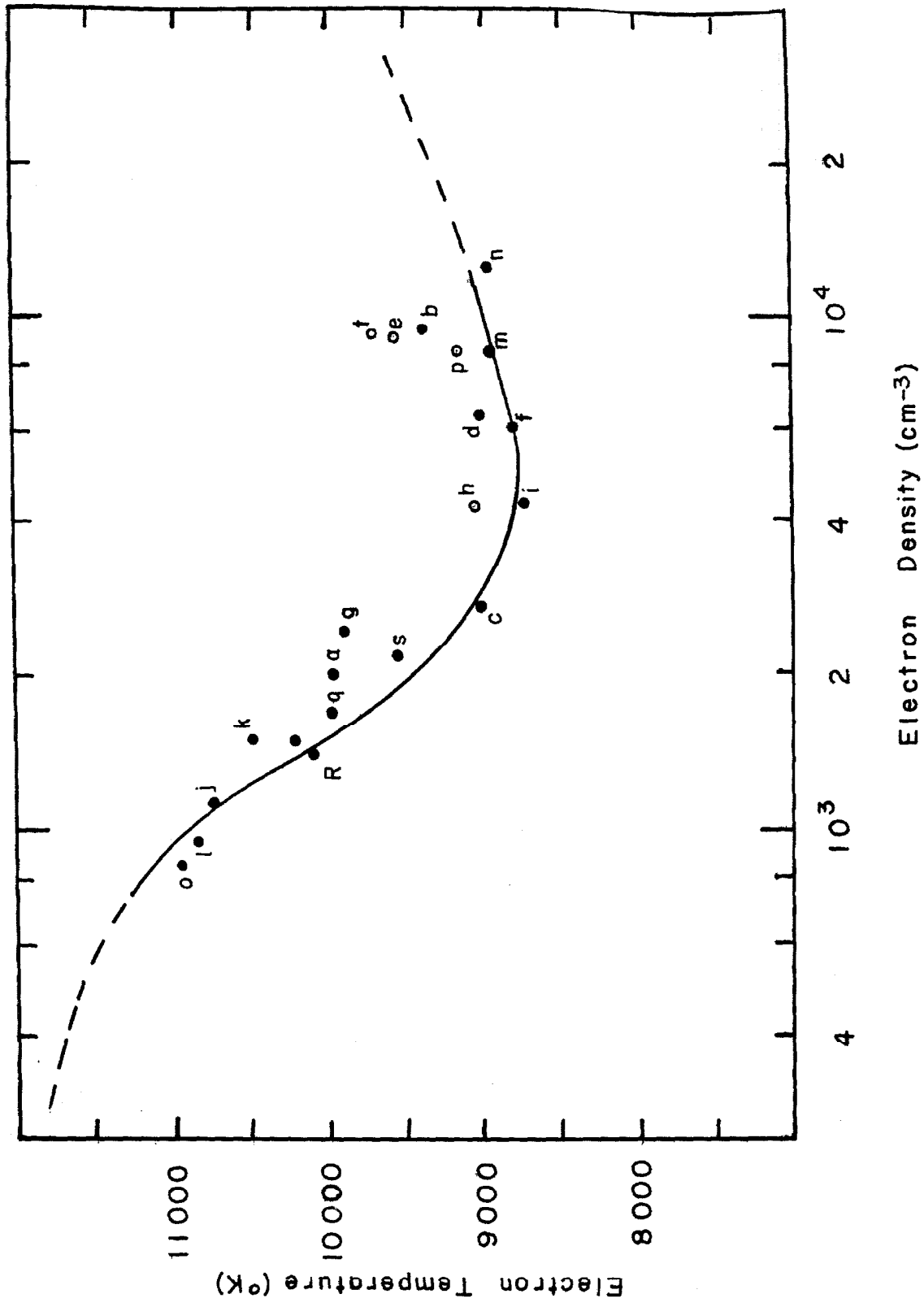
Electron Temperature (°K)
11000
10000
9000
8000
Electron Density (cm⁻³)
4
10³
2
4
10⁴
2
o
l
j
k
R
q
a
g
s
c
h
i
f
d
p
e
m
b
e
t
n

The ratio r was obtained from several points in the nebula. The line λ4363 was measured in units of the nearby line of helium at λ4388. Since the intensity of the latter line is known in units of H_β, λ4363 can also be measured in the same units. The other two lines, λ5067 and λ4959, being close to H_β, and of comparable intensity, can be directly obtained in the right units. Table XVI gives the values of the ratio for the points marked in Figure 1. The temperature obtained in this way is plotted against Ne in Figure 11. The values of the electron density are those given by Equation 50. More points can be included, however since all of them show the same behavior, only a few are presented, in order to avoid confusion in Figure 1.

TABLE XVI

Point	I(4363)	$Ne(r)x10^{-3}$	$Te^\circ K$
a	1.05	2.1	10 000
b	1.9	7.4	9500
c	1.45	2.7	9000
d	2.05	6.2	9100
e	1.70	9.0	9600
f	1.60	5.8	8800
g	1.50	2.6	9900
h	1.38	4.1	9100
i	1.30	4.3	8700
j	1.10	1.1	10 800
k	1.10	1.5	10 550
l	1.15	0.95	10 900
m	1.72	9.0	9000
n	1.78	13	9100
o	1.15	0.85	10 900
p	1.97	8.2	9300
q	0.78	1.7	10 100
r	0.75	1.4	10 100
t	1.31	2.1	9800
s	1.40	8.8	9600

The shape of the curve clearly demonstrates that the cooling mechanisms, operating in the nebula, do indeed depend on electron density. Moreover, as Daub's(55) computations indicate, the minimum of the curve depends on the stellar temperature, and consequently the value of that quantity could be determined. Daub's calculations contain an arithmetical error (see his Equation 19) and his results might be seriously affected by that. When his data is used, a temperature of about 45 000 K is derived for the exciting star. However, the variation of Te with density, as shown in Figure 11, to the left of the minimum, is much steeper than that predicted by the Daub theoretical calculations. Therefore, nothing can be said about what the cooling effect of dust might be, until more accurate calculations are carried out.

The shape of the curve can be explained qualitatively in the following manner. In the Orion nebula, the main source of kinetic energy of free electrons is provided by the photoionization of both hydrogen and helium. Those electrons, by collisions with each other and with impurities as well, establish a kinetic temperature. The value of this quantity depends on the rate of energy losses, which arise in the conversion of kinetic energy into radiation that escapes from the nebulae; this conversion occurring through free-free transitions and collisional excitation of the metastable levels of ions, like OII, OIII, SIII, etc. which

produce the forbidden lines. The most efficient element in this conversion is oxygen and OIII, having the strongest lines, is the most effective cooling agent. In the regions close to the center, OIII is the most abundant ion and consequently they are colder than the outer regions, where the oxygen exists mostly in the triple ionized stage; and the intensity of the OIII lines becomes weaker, consequently the temperature increases. For the innermost regions, where the electron density is higher than 10^4, there seems to appear a rise in temperature, probably due to the fact that OIII decreases again by recombination, and also because the S is mostly in the double stage of ionization. In any case, the curve is not as steep as Daub's computations predict.

It must be borne in mind that the density, plotted in Figure 11, corresponds to a spherically symmetrical nebula, with the electron density decreasing smoothly outwards. Then, condensations like r and q in the figure, which have 2.3 times the density corresponding to their positions in the symmetrical nebula, depart from the curve drawn. This departure can be explained by the vicinity of θ^2Ori; its radiation field must determine the thermal balance in those objects, rather than the one produced by the more distant θ^1C. On the other hand, points like s and h, having smaller surface brightness than their surroundings, should also have densities lower than those of the nebula with smoothly varying density. Figure 12 shows the corresponding variation

Figure 12

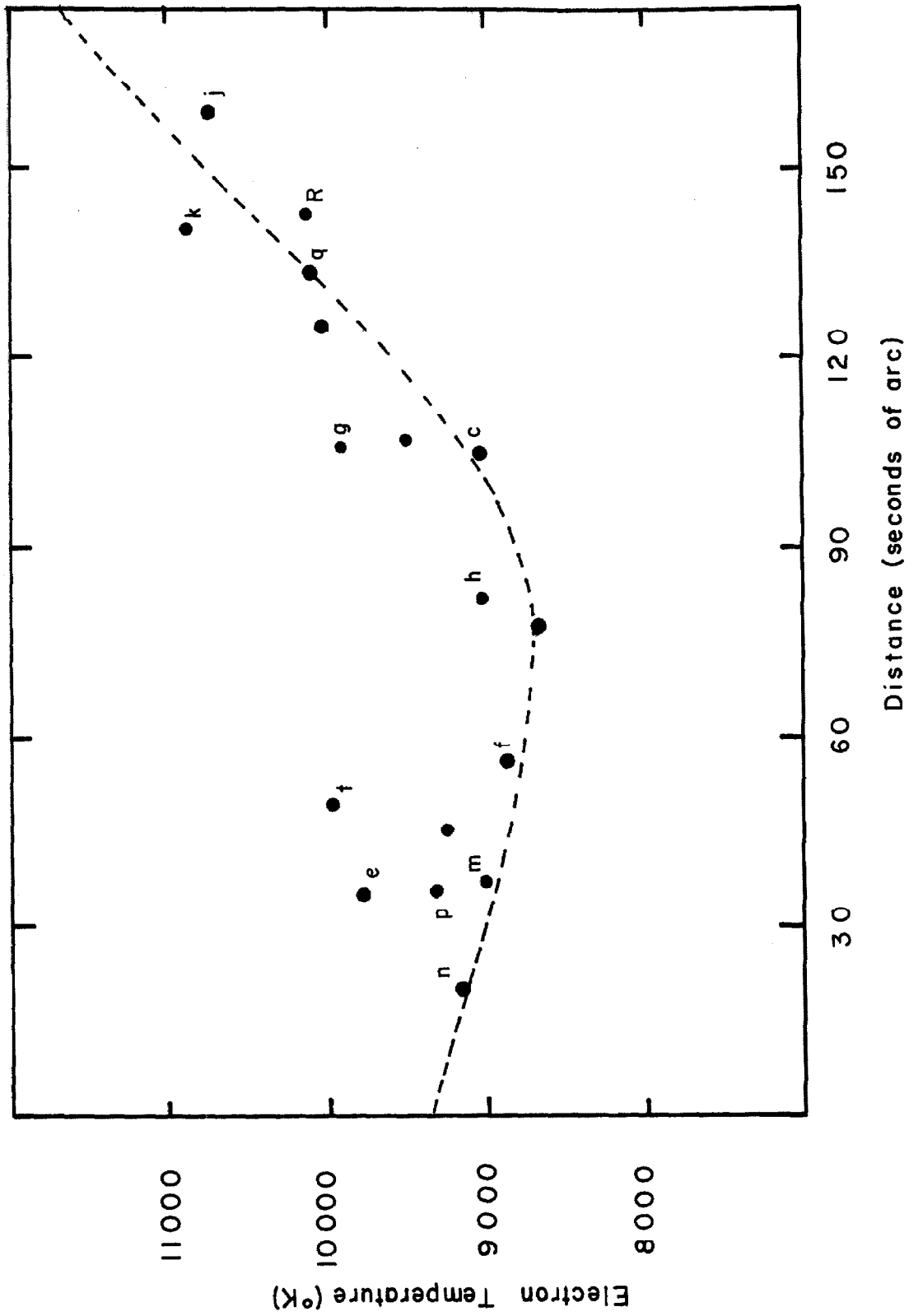
Electron Temperature (°K)
11000
10000
9000
8000
Distance (seconds of arc)
30
60
90
120
150
j
k
R
q
g
c
h
f
t
e
p
m
n

in electron temperature as a function of the distance from the center of the nebula.

c) The Abundance of Elements

The problem of determining the abundance of elements in a nebula is in principle much simpler than the corresponding one in stellar atmospheres. The ionic abundances are directly proportional to the line intensities, and if the atomic parameters are known, namely collisional cross-sections and transition probabilities, the constant of proportionality can be computed. When the relevant parameters are known by precise quantum mechanical computations, the accuracy that is obtained in the abundance determination is superior to that determined through analysis of stellar spectra. Unfortunately, the collision cross sections are known in only a few cases and approximate extimates must be made, which introduce large uncertainties. Another source of uncertainty is given by the fact that the radiation field in the nebula is not well known; black body approximations are used when the ionization equilibrium equation is needed to determine the contribution of the different stages of ionization of a given element. However, this latter limitation is not very serious, since some elements show lines from two or even three stages of ionization. Consequently, interpolation of the results obtained with those elements can be used for ions with stages of ionization that do not present emission lines. The atoms used in the

present investigation to determine the ionization equilibrium are: [OI], [OII], [OIII], and [SII] and [SIII], which present lines in the visible region. All the analysis presented here refers to the data obtained from point 1, from photoelectric and photographic material.

The electron density for point 1 is close to 10^4; this relatively low value permits us to make certain simplifications to the problem of the abundance determination from line forbidden emission, since we can neglect the existence of term 3. Similarly the number of collisional excitations of term 2 can be estimated and compared with A_{21}.

Equation 67, for Te = 10 000 K and Ne = 10^4 is

$$q_{21} = 8.63 \times 10^{-4} \frac{\Omega(1,2)}{(2J_2+1)}$$

Since the collision strength is of the order of unity for all the transitions considered here, we have to consider the deactivation rate only for OII and SII, the transition probabilities A_{21}, which are compatible to q_{21}. For all the other 2-1 transitions the q_{21} can be safely neglected. With this simplification, for an element X, which produces the emission line (s) at λ, the intensity ratio of $I(\lambda)$ to $I(H_\beta)$ is given by:

$$r(\lambda) = \frac{I(\lambda)}{I(H_\beta)} = \frac{N(X)}{N(H)} \frac{8.63 \times 10^{-8} p \, N_e \Omega}{a_{1,2} \, N_e (2J_1+1)} \frac{0.4861}{\lambda} e^{-\frac{1.44}{\lambda}}$$

where λ is given in microns and p is the ratio of A_{21} to the

total rate of depopulation of term 2. The relative abundance is then given by

$$\frac{N(X)}{N(H)} = 7.14 \times 10^{-7} \frac{\lambda}{p\Omega} \gamma(\lambda) (2S_1+1) e^{\frac{1.44}{\lambda}} \qquad (74)$$

all the relevant data used in this work is given in Table 17, where the non-forbidden lines, produced by recombination, λ4267 of CII and λ3856 of SiII, are also included:

TABLE XVII

Ion	λ	$\gamma(\lambda)$	$\Omega(1,2)$	p	Ref.
CII	4267	0.47	rec.	-	(56)
NII	6583	51.0	2.17	0.75	(58)
OII	3726-29	130	1.28	0.68	(58)
OIII	5007	365	1.73	0.75	(58)
NeIII	3869	23.2	0.76	0.77	"
SiII	3856	0.08	rec.	-	(56)
SII	7316-30	7.6	2.02	0.70	(58)
SIII	9069	33.2	3.2	0.28	"
AIII	7135	8.2	0.91	0.80	"
AIV	4740	0.15	9.85	0.89	"
FeII	4287	0.22	1.1	0.35	(56)
FeIII	4658	1.0	0.8	0.41	(58)

The lines of CII and SiII require the knowledge of the effective recombination coefficients. The value of these quantities can be estimated from the tabulation of those coefficients given by Allen(56). The following values

were adopted as upper limits.

$$a(4^2F^\circ - 3^2D) = 1.2 \times 10^{-13} \quad \text{for CII}$$
$$a(4^2P^\circ - 3^2D) = 0.3 \times 10^{-13} \quad \text{for SiII}$$

The most abundant stage of ionization of C must be the second; so the abundance derived here refers only to CIII. For Si, the third state is still of significance; then the following relation was adopted,

$$N(Si) \approx N(Si\,III) + \frac{N(O\,III)}{N(O\,II)} N(Si\,IV) \quad . \quad (75)$$

The collisional strengths are not known for FeIII, nor for FeII. Rough estimates must be made of those quantities. The line of FeIII, occurring through the $a^3F_4 - a^5D_4$ electric quadrupole transition, involves a spin change collision. Those kinds of collisions can only occur by electron exchange, that is through the process:

$$A + l \longrightarrow B + l' \quad (76)$$

where l and l' are the angular momentum of the free electron before and after the collision. The conservation theorem due to Moth, Bohr, Peierls and Plosczek, which state that

$$\sum \frac{\Omega_a}{(2J_a+1)} \leq (2l+1) \quad (77)$$

(the summation must be carried out over all levels of the ground configuration) is specially useful for setting an

upper limit to the collision strengths. Moreover, Van Regemorter(59) has shown that $\Omega(i,j)$ is proportional to the corresponding quadrupole transition strengths, which in turn are directly proportional to the spontaneous transition probabilities. Gargstang(57) has carried out extensive computations for the FeIII ion, and the Aqij's are provided by his work. There are 12 lines arising between the $3F_4$ and $^5D_4$ terms; consequently, through the corresponding optical transition probabilities, one can weigh the various Ω's. By assuming that the main contribution to the collisions is produced by s electrons, the value of Ω, given in Table XVII, was derived.

The ionization potential of FeII is 16.2 ev., so one can expect small contributions from this stage of ionization. Consequently, the value of Ω is not very important and has been, more or less, arbitrarily set at unity. The contribution from FeIV, which does not show up any lines, has been estimated using Equation 75. Table XVIII shows the results obtained for the chemical composition of the Orion nebula. There is a remarkable agreement with the abundance derived from stars of the vicinity, a fact already pointed out by Aller(4). The only serious discrepancy is that shown by carbon, however the nebular determination could not be off for more than a factor of 1.6. Magnesium has been tentatively included from the analysis of 22 Ori(60). Table XVIII also gives the corresponding solar abundance

values as derived by Aller and Goldberg(61).

TABLE XVIII

Element	Orion Neb.	Sun	22 Ori	Uncertainty Factor
H	10^6	10^6	10^6	-
He	91 000	-	-	1.08
C	1100	530	220	1.6
N	35	100	60	1.8
O	290	900	400	1.3
Mg	100	25	115	-
Ne	70	-	-	1.5
Si	50	32	85	1.5
S	20	20	25	1.3
A	4.0	-	-	2.0
FeII+FeIII	1.9	-	-	1.6
Fe	3.9	3.2	-	2.0

The only major discrepency is that indicated by the C/N ratio, which is about 7 times higher than for 22 Ori and the Sun. It is interesting to point out that the ratio by number of helium atoms to heavier elements is 52 which is fairly close to the value of 60 derived from the solar cosmic rays observed after the flare on November 5, 1960, as measured during three rocket flights(62). The abundance by mass is then:

$$Z = 0.02; \quad Y = 0.26; \quad X = 0.72.$$

d) The [SII] Lines

The forbidden lines of sulphur are particularly valuable because they can provide a method of determining the electron density. Czyak and Krueger(62) have carried out extensive calculations for computing the transition probabilities of several ions. The results obtained in the past for [SII] have thereby been improved. Although the values of the transition probabilities computed by the above mentioned authors are quite accurate, the corresponding collision strengths are only estimates. The electron densities derived from the [SII] are always much higher than the values derived by other methods; the discrepancy has been explained in terms of inhomogeneities; that is, by assuming the existence of condensations where the electron density is much higher than in the surroundings. The observed ratios obtained in this work provide the opportunity of checking the validity of the explanation given. With the parameters published and for point 1, where the density is not higher than 1.5×10^4, the [SII] lines indicate a density of about 60 000, which cannot be accepted, for otherwise the amount of absorption should be increased by a factor of at least 30, or about 3.7 magnitudes, which is far too high.

An empirical determination of the collisional cross-sections has been carried out using the intensity ratios:

$$r = \frac{I(6716 + 6730)}{I(4068 + 4076)} \quad \text{and} \quad r' = \frac{I(6716)}{I(6730)}$$

The first ratio is given by

$$r = \frac{b_2(N_e,T_e)}{b_3(N_e,T_e)} \frac{\left[\frac{6\,A_{6716}}{6716} p_{1c}(N_e) + \frac{4\,A_{6730}}{6730} p_{3a}(N_e)\right]}{\left(4\,\frac{A_{4068}}{4068} + 2\,\frac{A_{4076}}{4076}\right)} \qquad (78)$$

where the $p_\lambda(Ne)$, which takes into consideration the deexcitation rate, has been included for the nebular lines only, because the transition probabilities are of the same order of magnitude as q_{21}, for the densities of the central parts of the nebula. The collisional deactivation rate is:

$$q_\lambda = 8.63 \times 10^{-4} \frac{\Omega(1,2)}{(2J+1)_{term}} \times \qquad (79)$$

where

$$x = N_e\, t^{-1/2}\, 10^{-4} \quad ; \quad t = 10^{-4} T_e$$

the p factors are for x = 1.4:

$$p(\lambda 6730) = 0.78$$
$$p(\lambda 6716) = 0.58$$

With these numerical values, Equation 78 becomes:

$$r = 3.76 \times 10^{-3} \frac{b_2(N_e, T_e)}{b_3(N_e, T_e)} e^{\frac{1.395}{t}} \qquad (80)$$

When the deexcitation rate from term 3 is neglected (as a first approximation) the other ratio is given by:

$$r' = \frac{\left[1 + \frac{8.64 \times 10^{-7}}{A_{6730}\, T_e^{1/2}} N_e \left\{\Omega(1,2) + \Omega(2,3) e^{-\frac{1.395}{t}}\right]\right.}{\left[1 + \frac{8.64 \times 10^{-7}}{A_{6716}\, T_e^{1/2}} N_e \left\{\Omega(1,2) + \Omega(2,3) e^{-\frac{1.395}{t}}\right]\right.} 1.5 . \qquad (81)$$

In the Orion nebula, for the point 1, the ratios are:

$$r = 1.15 \pm 0.15 \quad \text{and} \quad r' = 0.64 \pm 0.05$$

If the density if taken as 1.4×10^4 and the temperature as 9500°K, one can solve Equations 78 and 79 by trial and error and obtain the values of $\Omega(1,2)$ and $\Omega(2,3)$. Once these quantities were determined, $\Omega(1,3)$ was changed and the process repeated. It was found that the most relevant parameter was $\Omega(2,3)$, both ratios are very sensitive to changes in this quantity, provided this parameter does not go beyond 50. The values found with this process are given in Table XIX, where the old parameters are also given.

TABLE XIX

	Seaton's Values	Estimated	
$\Omega(1,2)$	2.02	1.89	± 0.20
$\Omega(1,3)$	0.38	0.43	± 0.10
$\Omega(2,3)$	12.70	39.8	± 7.62

With the new collision strengths, Equation 81 is then

$$\gamma' = 1.49 \; \frac{1 + 0.086x(1+21.5\epsilon)}{1 + 0.332x(1+21.5\epsilon)} \qquad (82)$$

where $x = 10^{-4} N_e t^{-1/2}$; $\quad \epsilon = e^{-\frac{1.395}{t}}$

Although the agreement with the densities, as determined from the [OII] lines, is much closer with the new

Figure 13

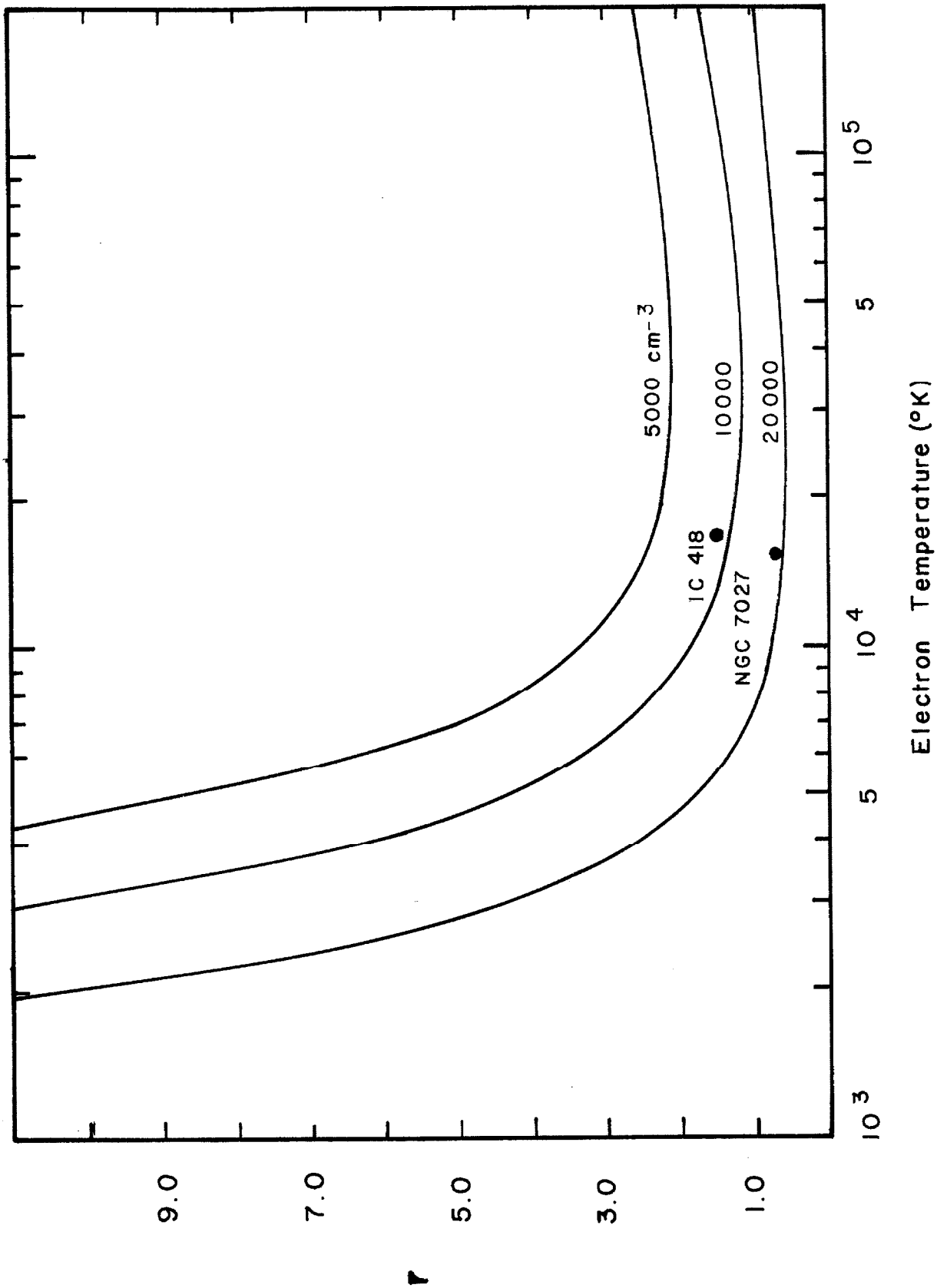
9.0
7.0
5.0
3.0
1.0
r
10^3
5
10^4
5
10^5
Electron Temperature (°K)
5000 cm^{-3}
10000
20000
IC 418
NGC 7027

parameters, there still seems to be an overestimation, of about 15 percent, in density when Equation 80 is used. However, the trial and error method is merely an approximation. When more observations of the [SII] lines, for other objects, are available, a more accurate formula can be derived following the same method used by Seaton and Osterbrock(63) for the [OII] lines.

The [SII] lines can be then used to determine the density through Equation 82; when this density is introduced in Equation 80, the value of the electron temperature can be derived. Figure 13 shows the variation of the ratio r as a function of electron temperature and for three different values of the electron density. Values of the ratios for two planetary nebulae are plotted for comparison. The ratios were obtained through photoelectric scans of the spectra of those nebulae(45). As can be seen from Figure 13, the ratio is sensitive for very low temperatures. With Te = 1.5 x 10^4, the ratio indicates an electron density of about 1.8 x $10^4 cm^{-3}$ for NGC 7027. For IC418 with Te = 1.7 x 10^4, which is the temperature indicated by the [OIII] lines, the density indicated, by Figure 13, is 0.85 x $10^4 cm^{-3}$.

e) Density Fluctuation Effects on the [OII] Lines

In section 6 of Chapter III, the character of the density fluctuations was established, namely that the nebula is more homogeneous close to center than in the outer regions. However, it was assumed that the density outside the conden-

sations was zero; this hypothesis was adopted in order to show that the apparent disagreement of the optical and radio observations can be satisfactorily explained in terms of density fluctuations. In order to make a more realistic estimate of the extent of those fluctuations, let us consider that the density outside the condensations is non-vanishing. Let N_e be the density of those condensations, and let N_e^1 be the density in the outside. Using an optical path αL for the condensations, and consequently $(1-\alpha)L$ for the path in between; for the ratio of the nebular to the auroral lines of OII we have

$$\frac{I(neb.)}{I(aur.)} = \frac{\Lambda_2(N_e)\,\alpha\, b_2(N_e) + (1-\alpha)\, b_2(N_e^1)\,\Lambda(N_e^1)}{\Lambda_3\left[\alpha\, b_3(N_e) + (1-\alpha)\, b_3(N_e^1)\right] e^{-\frac{1-\alpha}{\lambda_a}}} \quad , \quad (83)$$

where the quantities Λ_2 and Λ_3 involve the transition probabilities, the wavelengths, the weight of the upper level, and the factor $p(N_e)$, which takes into account the collisional deexcitation;

$$\Lambda(N_e) = \sum_1 \frac{A_{n1}\, w_n}{\lambda_n}\, p_n(N_e) \quad , \quad (84)$$

The summation is carried over all possible lines; λ_a is the mean wavelength of the auroral lines. All calculations have been carried out for an electron temperature of 10^4 K. For the oxygen lines, introducing numerical values, one has:

$$\Lambda_3\,(OII) = 1.41 \quad .$$

Since the densities involved are very small, the deactivation coefficient p can be taken as unity. That is not the case for the second term, since the lines arising from the corresponding levels have transition probabilities of the same order of magnitude as the collisional deactivation rate, then

$$\Lambda_2(N_e) = (193\, p_{3726} + 68.5\, p_{3729})10^{-5}. \quad (85)$$

Table XX illustrates the variation of Λ_2 as a function of density.

TABLE XX

x	$\Lambda_2(N_e)\times10^3$
1.4	1.22
1.0	1.17
0.5	1.74
0.1	2.37
0.05	2.48
0.0	2.61

Equation 83 can now be rewritten as:

$$\frac{I(neb.)}{I(aur)} = 5.08\, \frac{\alpha(\gamma)\Lambda(N_e)b_2(N_e) + (1-\alpha(\gamma))\Lambda(N_e^1)b_2(N_e^1)}{\alpha(\gamma)\, b_3(N_e) + [1-\alpha(\gamma)]\, b_3(N_e^1)}. \quad (86)$$

In Equation 86, there are three variables involved - $\alpha(\gamma)$, N_e, and N_e^1. The value of the electron density inside the condensations is given by the observations of the 3726-29 lines carried out by Osterbrock. The value of N_e^1,

Figure 14

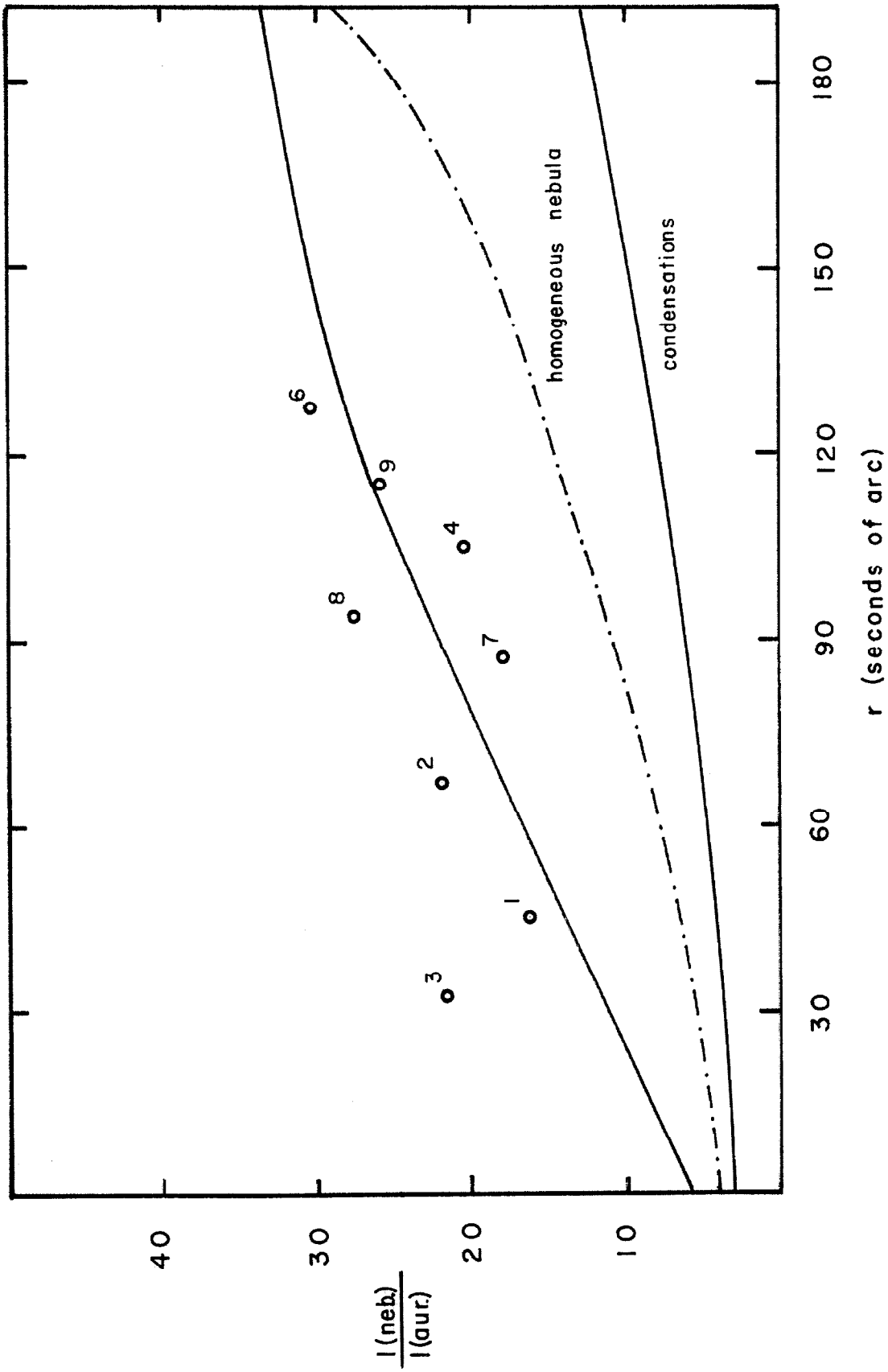
40
30
20
10
I(neb.)/I(aur.)
30
60
90
120
150
180
r (seconds of arc)
homogeneous nebula
condensations
1
2
3
4
6
7
8
9

the density outside the condensations, was fixed by trial and error until the variation in the ratio, as determined by the observations, was closely matched. The value of α must be smaller than that given in section III-6 because now the electron density in the space between the condensations is not zero; then α was taken as:

$$\alpha(r) = \alpha_o(r) \frac{N_e}{N_e}^{1} \qquad (82)$$

where α_o is the value given in III-6. The variation in temperature was not considered because it is not very important for the range of temperatures found in the nebula. In any event, a change of 1000°K will alter the value of the ratio by less than 10 percent, which is within the limit of the observational errors. Table XXI gives the results. The ratios corresponding to a nebula with a smooth density distribution are also given. Figure 14 shows the comparison with the observed ratios. The ratios corresponding to the condensations are also plotted, to stress the fact that the Orion nebulae do indeed contain density fluctuations.

TABLE XXI

Distance	X	X'	α^{-1}	γ	$X_{S.N.}$	$\gamma_{S.N.}$
0	1.8	0.3	6	6.9	1.4	3.5
1'	1.05	0.2	15	16.1	0.61	7.1
2'	0.58	0.08	97	28.0	0.23	15.2
3'	0.31	0.03	230	32.3	0.09	23.4

REFERENCES

1. Mathis, S.J. 1957, Ap.J., 125, 328.
2. Greenstein, J.L. 1946, Ap.J., 104, 414.
3. Aller, L.H. and Liller, W. 1959, Ap.J., 130, 45.
4. Andrillant, Y. and Andrillant, H. 1959, Ann. Ap., 22, 104.
5. Osterbrock, D. and Flather, E. 1959, Ap.J., 129, 26.
6. Münch, G. and Wilson, O.C. 1962, Z.Ap., 56, 127.
7. Würm, K. 1961, Z.Ap., 52, 149.
8. Wilson, O.C., Münch, G., Flather, E.M., and Coffeen, M.F. 1959, Ap.J. Suppl. 4, 199.
9. Münch, G. 1963, A.J., 68, 287.
10. Oke, J.B. 1960, Ap.J., 131, 358.
11. Flather, E. and Osterbrock, D. 1960, Ap.J., 132, 18.
12. Code, A. 1959, Compendium of Astronomy, Vol. 6, Chap. 2.
13. Ambartzumian, V.A. 1933, Z.Ap., 6, 107.
14. Strömgren, B. 1951, Problems of Cosmical Aerodynamics, (Dayton, Ohio) Chapter 2.
15. Würm, K and Grubisich, C. (to be published).
16. Divan, L. 1954, Ann. Ap., 17, 456.
17. Borgman, J. 1960, B.A.N. 15, 255.
18. Baade, W. and Minkowski, R. 1937, Ap.J., 86, 123.
19. Stebbins, J. and Whitford, A.E. 1945, Ap. J. 102, 318.
20. Mathis, J.S. 1962, Ap.J., 136, 374.
21. Burgess, A. 1958, M.N., 118, 477.
22. Van de Hulst, H.C. 1949, Rech. A. Obs., Utrech 11, Pt II.

23. Wilson, O.C. 1956, P.A.S.P. 68, 346.

24. Seaton, M. 1960, M.N., 120, 326.

25. Baker, J.G. and Menzel, D.H. 1938, Ap.J., 88, 52.

26. Seaton, M. 1959, M.N., 119, 90.

27. Searle, L. 1958, Ap.J., 128, 489.

28. Menon, T.K. 1958, Ap.J., 127, 28.

29. Pottasch, S.R. 1960, Ap.J., 131, 702.

30. Struve, O., Wurm, K. and Menyey, L.G. 1939, Proc. Nat. Acad. Sci. 25, 67.

31. Osterbrock, D. 1962, Ap.J., 135, 195.

32. Unno, W. 1952, P.A.S. Japan, 4, 100.

33. Chamberlain, J.W. 1953, Ap.J., 117, 387.

34. Osterbrock, D., Capriotti, E.R. and Bautz, L. 1963, Ap.J., 138, 62.

35. Capriotti, E.R. 1963, Ap.J., in press.

36. Mathis, J.S. 1957, Ap.J., 125, 318.

37. Burgess, A. and Seaton, M.J. 1960, M.N., 121, 471.

38. Pottasch, S.R. 1962, Ap.J., 135, 385.

39. Wilson, O.C. 1940, Ap.J., 91, 360.

40. Huang, Su Shu 1948, Ap.J., 108, 354.

41. Seaton, M.J. 1955, Proc. Phys. Soc. 68, 457.

42. Pariiskii, Y.N. 1962, Soviet A.J., 5, 611.

43. Faulkner, D.J. 1963, Roy. Ast. S.Q., 4, 235.

44. Aller, L.H. and Faulkner, D.J. 1962, P.A.S.P., 74, 219.

45. O'Dell, C.R. 1963, private communication.

46. Menon, T.K. 1961, Pub. of N.R.A.O., 1, 1.

47. Sharpless, S. 1962, Ap.J., 136, 767.

48. Sharpless, S. 1952, Ap.J., 116, 251.

49. Lilley, E. 1955, Ap.J., 122, 197.

50. Seaton, M. 1960, Rep. Prog. Phys., 23, 311.

51. Barbier, D. 1944, Ann. Ap., 7, 80.

52. Kahn, F.D. and Menon, T.K. 1961, Proc. Nat. Acad. Sci., 47, 1712.

53. Hayashi, S. 1961, P.A.S. Japan, 13, 450.

54. Smerd, S.F. and Westfold, K.C. 1949, Phil. Mag., 40, 831.

55. Daub, C.T. 1963, Ap.J., 137, 184.

56. Allen, C.W. 1963, Astrophysical Quantities.

57. Gargstang, R.H. 1957, M.N., 117, 393.

58. Aller, L.H. 1956, Gaseous Nebulae.

59. Van Regemorter 1962, Ap.J., 136, 906.

60. Aller, L.H. 1960, Vol. VI of Kuiper Compendium, Page 219.

61. Aller, L.H., Goldberg, L. and Müller, E. 1960, Ap.J. Suppl. 5, 1.

62. Buswas, S., Fitchel, C., Guss, D. and Waddington, C. 1963, J.G.R., 68, 3109.

63. Czyzak, S.J. and Kmegen, T.K. 1963, M.N., 126, 177.

64. Seaton, M.J. and Osterbrock, D. 1957, Ap.J., 125, 66.